THE USE OF FD-FILAMENTOUS BACTERIOPHAGE FOR THE *IN VIVO*

IMAGING OF CANCER

A Thesis presented to the Faculty of the Graduate School

University of Missouri-Columbia

In Partial Fulfillment

Of the Requirements for the Degree

Master of Science

---

by

JESSICA R NEWTON

Dr. Susan L. Deutscher, Thesis supervisor

DECEMBER 2006

The undersigned, appointed by the Dean of the Graduate School,
have examined thesis entitled

THE USE OF FD-FILAMENTOUS BACTERIOPHAGE AS A BIOLOGICAL
NANOPARTICLE FOR THE *IN VIVO* IMAGING OF CANCER

Presented by Jessica R. Newton

A candidate for the degree of Master of Science

And hereby certify that in their opinion it is worthy of acceptance.

_____
Professor Susan L. Deutscher

_____
Professor Thomas P. Quinn

_____
Professor George P. Smith

ACKNOWLEDGEMENTS

TABLE OF CONTENTS

Chapters

Introduction
Bacteriophage Display and Cancer Imaging
Purpose of the Study

Introduction
Materials and Methods
Results
Discussion

Introduction
Materials and Methods
Results
Discussion

LIST OF ILLUSTRATIONS

Figure   **Page**

LIST OF TABLES

Table		Page

LIST OF ABBREVIATIONS

^{111}In-SA, ^{111}In-DTPA-streptavidin

AF680, Alexa Fluor 680$^{®}$

α-MSH, alpha-melanocyte stimulating hormone

cp, coat protein

CT, Computerized Axial Tomography

DMEM, Dulbecco's modified Eagle's medium

DTPA, diethylenetriaminepentaacetate

E. coli, *Escherichia coli*

FBS, fetal bovine serum

HEK, human embryonic kidney

HEPES, 4-2-hydroxyethyl-1-piperazineethanesulfonic acid

IU, infectious units

MBq, megabecquerel

MC1R, melanocortin 1 receptor

NIRF, near infrared fluorophores

PBS, 1X Dulbecco's PBS, Ca^{2+} and Mg^{2+} free

PEG, polyethylene glycol

PSA, prostate specific antigen

SA, streptavidin

SCID, severe combined immune deficiency

SPECT, Single photon emission computed tomography

SPCH, selected prostate carcinoma homing

TBS, tris buffered saline

WT, wild type fd

THE USE OF FD-FILAMENTOUS BACTERIOPHAGE FOR THE *IN VIVO* IMAGING
OF CANCER

Jessica R. Newton

Dr. Susan L. Deutscher, Thesis Advisor

ABSTRACT

Improved diagnosis of cancer through targeted imaging of neoplasms is needed for early detection and treatment of cancer. We propose that the physical characteristics of filamentous bacteriophage (phage) are well suited for use in the targeted imaging of cancer. This study describes the development of two different phage-based cancer imaging agents. One is specific for prostate carcinoma, and the other specific for melanoma, with each utilizing different imaging modalities - optical imaging and radioimaging.

A human PC-3 prostate carcinoma was optically imaged using phage displaying a newly selected prostate homing peptide labeled with the near infrared fluorophore AF680, whereas, a mouse B16-F1 melanoma was radioimaged using single-photon-emission-computed-tomography through a two-step pretargeting procedure. This pretargeting strategy utilized bifunctional bacteriophage that were both biotin labeled and displayed α-melanoma stimulating hormone peptide analogs and included streptavidin-chelator complex radiolabeled with ^{111}In. The successful imaging of prostate carcinoma and melanoma with different strategies exhibits the versatility of phage and highlights their utility in the imaging of cancer.

CHAPTER 1

INTRODUCTION

Cancer is a leading cause of death within the United States of America. The death rate due to cancer has not changed significantly since 1950, while heart disease mortality has decreased 40% in the same period. Consequently, cancer has now surpassed heart disease as the primary cause of death in people younger than 85 years old (*1, 2*). The development and progression of cancer is very complex, accordingly, the prevention and control of cancer will require a vast multidisciplinary effort. One of the major barriers for the reduction of cancer mortality rates is the inability to find and diagnose small primary cancers and/or metastatic lesions (*3*). Another patient health issue is the systemic use of traditional non-specific methods of treatment, such as chemotherapy and radiotherapy, which often cause acute toxicity and/or secondary tumors within the patient (*4, 5*). Thus, there has been a push to develop new and improved high throughput screening techniques to identify new cancer specific targeting compounds for potential use in diagnostics and/or therapeutics.

The resultant expansion and improvement of high throughput techniques has increased interest in "personalized treatment" of cancer (*6*) through the targeted delivery of imaging agents and/or therapeutics. The ability of an injected compound to target a tumor is a direct consequence of the affinity and specificity for the tumor, the rate of clearance from the blood and non-target tissues, as well as other physical characteristics (*7*). All of these characteristics are important factors that must be considered in the

development of tumor targeting imaging agents. It is envisioned that the evolution of low cost, reliable tumor specific imaging agents would not only greatly increase early diagnosis, but also facilitate the targeted delivery of therapeutics and thus improve the probability of survival.

BACTERIOPHAGE DISPLAY AND CANCER IMAGING

Bacteriophage (phage) are viruses that replicate by infecting bacteria and making use of some or all of the host machinery. Phage possess very small, simple, easily manipulated genomes. Smith and coworkers utilized class Ff filamentous phage to develop a high throughput combinatorial system that is now called phage display (*8*). In this system a library of random peptides are genetically fused with a coat protein so that they are displayed on the surface of the phage particle (or virion), allowing for the binding and, thus, the selection of peptides with high affinity for a given target. There are two types of phage display libraries commonly used for selection purposes, f88-4 and fUSE5 (Figure 1). The phage constructs produced with both of the libraries have a tetracycline resistance gene added to the phage genome for selection purposes. In the fd-tet f88 vector there are about 100 copies of the foreign peptide displayed on the major coat protein VIII (cpVIII), which forms a tubular sheath encasing all but the very tips of the long, thin virion. The fUSE5 vector contains up to five copies of the foreign peptide within coat protein III (cpIII), which is located at one tip of the virion.

The ability of phage to display multiple copies of a tumor targeting peptide makes them inherently multivalent. Thus the avidity of phage displaying multiple copies of a

2

tumor targeting peptide for its target would be greatly increased, compared to that of a single synthetic peptide (*9, 10*). Phage also possess thousands of cpVIII decorating the outer surface of the virion providing ample sites for covalent attachment of reporter molecules to the exposed N-termini of cpVIII. Increased avidity of modified phage for its target, coupled with the easily derivatized cpVIII encasing the length of the virion, makes the use of phage as an imaging agent an attractive prospect.

The use of phage as an imaging agent has many benefits. First and foremost is affordability and speed. The ability to easily manipulate the phage genome as a vector allows for quick modification and introduction of a foreign peptide to be displayed on the surface of the virion, compared to the more costly and lengthy procedure of peptide synthesis. Another consideration for the use of phage tagged with imaging labels is that after the phage display selection of many peptides, screening of the resultant recombinant phage particles allows for more flexibility than screening of the synthesized peptides. Initial screening of phage displaying selected peptides can be accomplished biologically by tracking the phage spectrophotometrically or by titering on host *E. coli*. More advanced screening and/or tracking of phage can be accomplished through the addition of imaging tags.

Addition of fluorophores, radiochelators, and epitope tags to a synthetic peptide can have negative effects on the peptide's binding properties (*11*). In comparison, phage contain thousands of easily derivatized cpVIII of which few to none would contain a tumor homing peptide. The sheer number of cpVIIIs could aid in the spatial separation of the displayed peptides and the chosen tag or label. Also, multiple labels covalently attached to the same virion have the potential to generate signal amplification. This

brightening effect would be useful for the *in vivo* characterization and development of potential tumor targeting peptides. Direct injection of labeled phage displaying tumor targeting peptides into a mouse model of cancer would allow for the noninvasive real-time imaging of the *in vivo* biodistribution, tumor targeting propensity, and clearance rate (*12*)of the labeled phage.

Phage directly radiolabeled with ^{131}I have previously been used to investigate wild type phage distribution within mice (*13*). However, utilizing directly radiolabeled phage for the development of tumor targeting imaging agents would not be advantageous. Due to the expense and technical difficulties of radiolabeling, as well as the possibility of radiation-induced bystander effects (*14, 15*). These issues have lead to considerable effort being placed on the development of new fluorescent probes capable of deep tissue *in vivo* optical imaging (*16-20*). Tissues and blood have a high transmittance and low scattering of near infrared photons (~650nm to ~900nm), thus, new near infrared fluorophores (NIRF) have been developed for *in vivo* optical imaging of tissues deeper than 0.5 cm (*21, 22*). These improved fluorophores along with advances in diffuse photon detection and increased knowledge of light propagation in tissue have lead to the ability for real-time detection and quantification of fluorescent signals *in vivo* (*23-26*).

Another technique to reduce possible bystander effects is to utilize a pretargeting strategy in which phage are labeled with an epitope tag and the radiolabel is appended to a smaller, faster clearing particle which recognizes and binds to the pretargeted epitope tag. One such system commonly used is based on streptavidin's very high affinity for biotin ($Kd=10^{15}$) (*27*). Paganelli and coworkers utilized biotinylated monoclonal antibodies and ^{111}In radiolabeled streptavidin to image ovarian cancer in human patients

(*28*).   This study as well as others has highlighted the utility of a pretargeted radioimmunotherapy approach (*27, 29*).   Using biotinylated phage in a pretargeting strategy should be beneficial as a single virion could be covalently attached to multiple biotins.   Multiple biotin molecules per virion would lead to a higher likely hood of streptavidin binding and possible signal amplification.

We hypothesize that the physical characteristics of fd filamentous bacteriophage are well suited for the delivery of tumor homing peptides and a diverse range of reporter molecules.

PURPOSE OF THE STUDY

In this study we utilize fd filamentous phage particles for the simultaneous delivery of targeting peptides and imaging/pretargeting tags for the *in vivo* imaging of tumor bearing mice.   In chapter two, phage displaying selected prostate carcinoma homing (SPCH) peptides were fluorescently labeled with the near infrared fluorophore (NIRF) Alexa Fluor 680[®] for the purpose of *in vivo* optical imaging of xenografted PC-3 human prostate carcinomas in severe combined immune deficiency (SCID) mice.   The use of the newly developed NIRFs and optical imaging techniques provides a safe alternative for diagnosis and observation of disease progression.   One drawback to the use of optical imaging is that it is a new technique and on the "cutting edge" and therefore its use is not immediately transferable to the clinical setting.   However, the more traditional route of disease imaging utilizes radioisotopes which can cause damage to surrounding tissues (*15*).

In chapter three, phage displaying melanoma homing peptides were biotinylated for the purpose of pretargeting syngeneic grafted B16-F1 mouse melanoma tumors in C57/BL6 mice. This study utilized a more traditional and more immediately applicable form of imaging with the use of radiolabels. In an effort to reduce background levels as well as possible damage to surrounding tissues, the biotinylated phage were pretargeted to the tumor and the radiolabel was appended to a smaller, faster clearing compound (streptavidin-DTPA). In each experiment phage successfully targeted and imaged the desired tumor target.

Figure 1: Schematic of fUSE5 and f88 phage display

f88-4 Phage Display Vector   fUSE5 Phage Display Vector

cpVIII

Modified
cpVIII

Modified
cpIII
Gene

Modified
cpVIII
Gene

Tetracycline
Resistance
Gene

cpIII
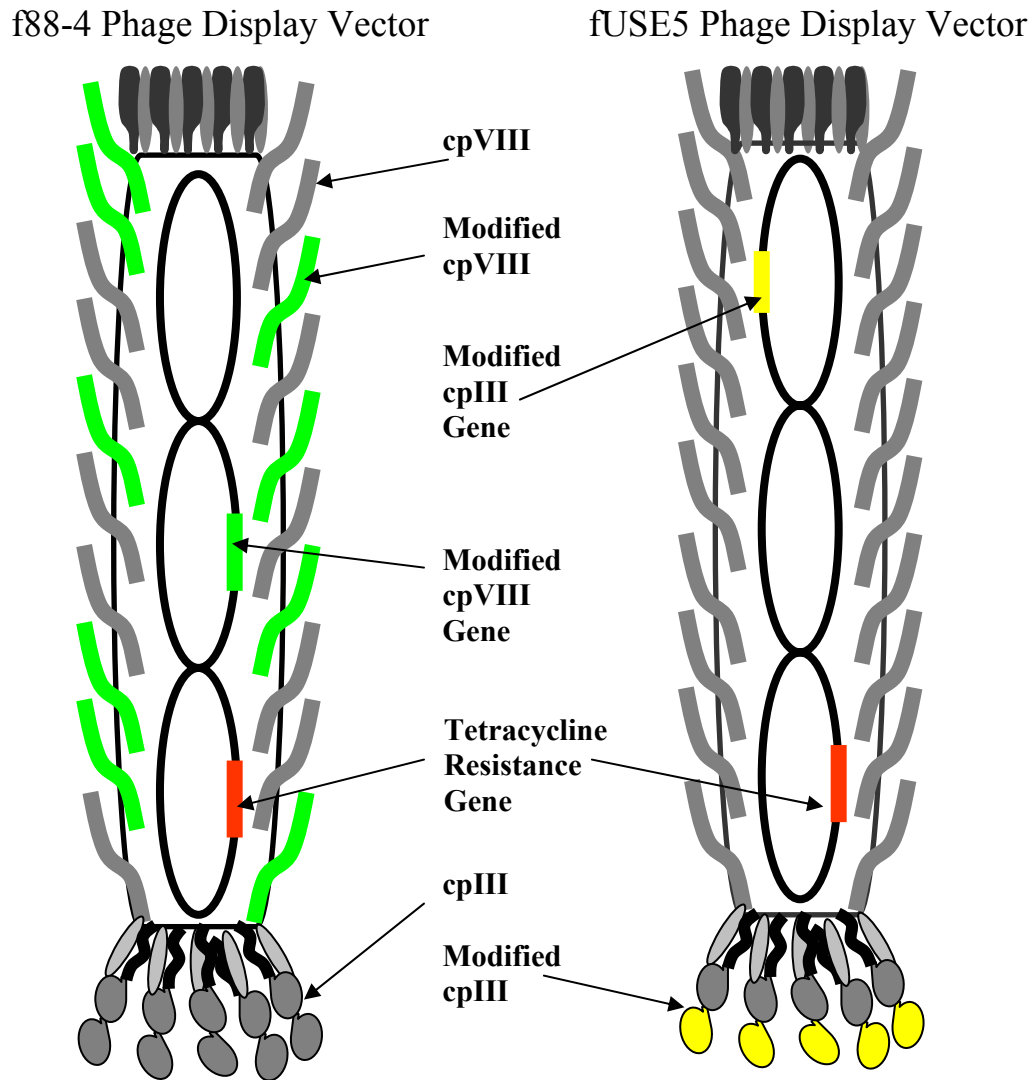
Modified
cpIII

This schematic presents two commonly used phage display vectors, f88-4 and fUSE5. Green highlighting is used to illustrate the gene encoding a modified cpVIII and the subsequent protein product within the f88-4 phage display vector. The fUSE5 phage display vector contains a modified cpIII gene and protein product which are highlighted as yellow. Each phage display vector has a tetracycline resistance gene (highlighted in red) incorporated into the genome for selection purposes.

7

FLUORESCENCE OPTICAL IMAGING OF CANCER

INTRODUCTION

The incidence of prostate cancer in men is second only to that of skin cancer in the United States and accounts for over 40,000 annual deaths (*2*). Although there is good evidence that prostate specific antigen screening can detect early-stage prostate cancer, it is nonspecific and can miss up to 30% of carcinomas (*30*). Furthermore, markers for distant prostate cancer metastases are needed. Recent efforts have focused on identifying new prostate cancer-specific cell surface antigens, receptors and other locally expressed biomarkers. Peptides, because of their ease of synthesis and often ideal pharmacokinetic characteristics as well as non-immunogenic nature, are attractive targeting agents for development of new prostate cancer imaging or therapeutic agents.

The display of peptide libraries on the surface of phage offers a way of searching for peptides with specific binding properties. *In vitro* phage display has been used to select peptides that target cancer-associated antigens (*31, 32*), while cultured carcinoma cells have also been employed to isolate peptides that bind a variety of human carcinoma cell lines (*33-35*). *In vivo* phage display selection procedures offer an advantage over *in vitro* screening protocols in that phage can be selected based on desired pharmacokinetic properties including delivery and tumoral accumulation. Recently, *in vivo* phage display has been explored as a means to identify phage and corresponding peptides with optimal tumor-targeting properties in the context of a living animal, however many of these

peptides bind to endothelial cell markers but not directly to tumor cells (*36, 37*). We believe *in vivo* selected phage can serve as valuable first-line agents to determine if the phage and corresponding synthesized peptides would function as efficacious tumor-targeting and imaging agents.

Here, we report an *in vivo* phage display selection protocol and a micropanning assay that allowed the identification of novel prostate cancer targeting peptides. The identified phage clones were able to extravasate from the endothelium and specifically target prostate cancer cells *in vivo*. More precisely, prostate tumor-avid phage were selected from a fUSE5 15-amino acid peptide library (*38*) in severe combined immune deficiency (SCID) mice bearing heterotransplanted human PC-3 prostate tumors. An innovative "tumor-to-cell micropanning" assay was used to distinguish phage with high affinity for prostate tumor tissue/heterotransplanted cell lines relative to normal tissues and cell lines. A single phage clonal population with high affinity for both prostate tumor tissue and PC-3 carcinoma cell lines was fluorescently labeled with the near infrared fluorophore (NIRF), Alexa Fluor 680 (AF680), and its ability to bind prostate carcinomas, both *in vitro* and *in vivo*, was analyzed. The AF680 labeled phage were specific for PC-3 cells *in vitro* and allowed the successful non-invasive imaging of prostate tumors in SCID mice.

MATERIALS AND METHODS

Materials: Cell culture reagents were purchased from Invitrogen (Carlsbad, California). All other chemicals were purchased from Sigma Chemical Company (St. Louis, Missouri), unless otherwise stated.

9

Cell lines: PC-3 cells (*39*) were grown in Ham's F12K media, 7% fetal bovine serum (FBS), 2 mM L-glutamine, and 48 μg/ml gentamicin at 37° C in 5% CO_2. Human embryonic kidney (HEK) 293 cells were cultured in Dulbecco's modified Eagle's medium (DMEM)-high glucose with 10% heat inactivated FBS, 2 mM L-glutamine, 1 mM sodium pyruvate and 48 μg/ml gentamicin at 37° C in 5% CO_2. All other cell lines were grown in a general maintenance media containing RPMI 1640 (custom) with 10% FBS, and 48 μg/ml gentamicin. The cell lines were tested for pathogens before injection into mice.

Mouse strains and handling: Four- to 6-week-old (approximately 20 grams) ICRSC-M SCID outbred mice were obtained from Taconic (Germantown, New York) and maintained in approved pathogen free institutional housing. Animal studies were conducted outlined in the NIH guide for Care and Use of Laboratory Animals and the Policy and Procedures for Animal Research at the Harry S. Truman Memorial Veterans' Hospital and Massachusetts General Hospital. Solid tumors were established in SCID mice over a period of four weeks resulting in mice with appropriately 1 cm sized tumors for all experiments. 5×10^6 PC-3 prostate carcinoma cells were injected subcutaneously in one flank of each anesthetized animal. Tumors generally appeared in 30 days. Following *in vivo* selections (next subsection) or biodistribution (see below), the mice were euthanized and tumors and organs were excised from the animals and handled as described in later sections.

***In vivo* selection of tumor-targeting phage:** The fUSE5 phage display library, which displayed random 15 amino acid peptides on cpIII, was a gift from Dr. George

Smith (*40*). Library amplification was conducted as decribed previously (*41*). The phage particle concentration in virions was determined spectrophotometrically and the amount of infectious units (IU) was determined by titering on *E. coli* K91 Blue Kan.

10^{12} IU of a 15 amino acid fUSE5 library suspended in PBS (1X Dulbecco's PBS, Ca^{2+} and Mg^{2+} free), was injected into the tail vein of normal, non-tumor-bearing CF-1 mice, for 15 minutes in order to preclear phage that bound to normal vasculature and other non-tumor antigens (*42*). The mice were then anaesthetized and blood (~ 3 ml) was obtained. Phage were isolated from the blood by PEG precipitation, amplified, purified and dialyzed, as described previously (*41*). Next, 10^{12} IU of the pre-cleared phage library was injected into SCID mice bearing PC-3 human prostate cancer cell xenografts. After one hour of *in vivo* phage circulation, the mice were sacrificed by cervical dislocation. The animals were perfused with 90 ml of PBS to facilitate phage elimination from the vasculature, organs and tumors removed, weighed and quick-frozen in liquid nitrogen. Prostate tumors were ground in DMEM with protease inhibitors (1 mM phenylmethylsulfonyl fluoride, 20 μg/ml aprotinin and 1 μg/ml leupeptin), and 0.5% bovine serum albumin (*43*) (DMPB) and washed three times by centrifugation at 6000 rpm. The pelleted lysate was resuspended in DMPB + 2.5% CHAPS to recover extravasated phage, and the recovered phage population recovered was used to infect fresh *E. coli* K91 Blue Kan host cells. A portion of the purified phage preparation (in PBS) was used as the input phage for the next round of *in vivo* selection. In total, four rounds of selection were performed. Between rounds, the foreign DNA inserts and encoded peptide sequence were determined for 10 random phage clones to gauge selection process and absence of contamination. The amino acid sequences of the

11

displayed peptides were deduced from the DNA sequence. Sequences from the selections were compared using Align, PIR, NiceBlast, gapped and PSI-BLAST search databases (*44, 45*) to identify the presence of consensus motifs or potential tumor targets to define clones for further analyses.

Micropanning assay: A newly described multistep "micropanning" assay was devised to quickly and efficiently identify clones that specifically recognized PC-3 tumor tissue and PC-3 human prostate carcinoma cells and, thus, had potential in *in vivo* PC-3 tumor targeting. In the first tier of micropanning, 1.5×10^7 IU of *in vivo*-selected phage clones were incubated at 4ºC for 2 hours with excised normal muscle tissue or PC-3 tumor tissue. The tissues were then washed five times with DMPB and bound phage were eluted from the tissue by using DMPB + 2.5% CHAPS. A ratio of phage titer in tumor tissue to phage titer in normal tissue was calculated. *In vivo*-selected phage clones that recognized tumor tissue with 1.5-fold specificity over normal tissue were assumed to have sufficient affinity and specificity for prostate tumor cells to warrant further investigation. In the second tier of the assay, phage were identified that specifically bound to cultured PC-3 cells versus a non-relevant control cell line. Nine phage clones identified in the first tier were incubated (similar to the first tier) with either intact PC-3 prostate carcinoma cells or with non-relevant control cells (HEK 293). Bound phage were eluted with DMPB + 2.5% CHAPS and a ratio was calculated of phage titer in PC-3 cells divided by phage titer in HEK 293 cells.

Conjugation of AF680 to phage: AF680 carboxylic acid, succinimidyl ester 5-isomer (Invitrogen, Carlsbad, California) was dissolved in dimethyl sulfoxide and added to a suspension of phage in 1X coupling buffer (0.5 M Na_3citrate, 0.1 M $NaHCO_3$, pH

adjusted to 8.5 with NaOH) at a 1:1 molar ratio of AF680:cpVIII (1% DMSO final concentration). This mixture was then incubated at room temperature for 4 hours in the dark. Subsequently, ethanolamine at 150 mM (pH adjusted to 9.0 with HCl) was added for 2 hours in the dark at room temperature. The samples were then PEG precipitated twice and dialyzed extensively against 50 mM Tris-HCl, 150 mM NaCl, pH 7.5 (TBS), to remove excess hydrolyzed AF680.

Determination of binding of AF680 labeled phage to PC-3 cells by modified Enzyme-Linked Immunosorbent Assay (ELISA): PC-3 carcinoma cells were grown to ~90% confluency in a tissue culture treated 96-well plate (TPP, Trasadingen, Switzerland). The growth media (previously described) was removed and new complete media with the appropriate concentration ($5x10^9$ to $1x10^{11}$ virions/ml) of AF680 labeled phage or unlabeled phage was added to the wells. The plate was incubated at 37^oC for 1.5 hours then washed with ice cold PBS multiple times. Cells and bound phage were then fixed to the plate by addition of PBS with 4% formaldehyde. Presence of phage was then probed by addition of a rabbit polyclonal anti-phage antibody (courtesy of George Smith). The plate was then incubated at room temperature for 1 hour and extensively washed with TBS. A secondary anti-rabbit antibody conjugated to horseradish peroxidase (Santa Cruz Biotechnology, Santa Cruz, California) was added and incubated at room temperature for one hour. The plate was washed with TBS + 1% Tween and liquid peroxidase substrate (2,2''-Azino-bis(3-ethylbenzothiazoline-6-sulfonic acid) was added and incubated for ten minutes at room temperature. Addition of 1% SDS was used to stop the reaction. The plate was then read on a µQuant Universal Microplate

Spectrophotometer (Bio-Tek Instruments, Winooski, Vermont) at an absorbance of 405nm, using an endpoint assay.

Confocal microscopy for determination of cell surface binding: Binding of the AF680 labeled phage to PC-3, PC-3M, LNCaP, DU145, RPWE-1, MDA-MB-435, and HEK 293 cells was determined using laser scanning confocal microscopy, as described previously (*46*). 1 x 10^4 cells were dried onto a microscope slide and blocked with 6% BSA in 10 mM Tris. The slides were incubated with wild type fd (*47*) or selected prostate carcinoma homing (SPCH) phage solutions ($1x10^{11}$ virions/ml phage in 10 mM Tris, pH 7.5, 1% BSA) for 1 hour in the dark, at room temperature. Comparison of AF680 phage binding and biotinylated peptide binding to PC-3 carcinoma cells and HEK 293 cells was also conducted using laser scanning confocal microscopy. Binding of biotinylated peptide (SPCH and scrambled SPCH) was detected by using 10 μg/ml NeutrAvidin-Texas Red (Molecular Probes, Eugene, Oregon) (incubation for 30 min at room temperature in the dark). Laser scanning confocal microscopy was performed on a Bio-Rad MRC 600 confocal microscope (University of Missouri Molecular Cytology Core Facility).

Biodistribution of AF680 labeled phage: AF680 labeled phage (~10^9 IU) were injected intravenously into SCID mice bearing PC-3 prostate cancer cell xenografts. The mice were sacrificed at 5 minutes, 30 minutes, 2, 4, 6 and 24 hours after injection. Mice were perfused with 90 ml of PBS and organs and tumors were removed and quick-frozen in liquid nitrogen. Organs and tumors were ground in TBS buffer, the amount of protein in each tissue homogenate was then determined using the Bio-Rad Protein Assay (Bio-Rad Laboratories, Hercules, California). Tissue homogenates at 5 mg/ml of protein were

14

analyzed for fluorescent activity at appropriate wavelengths, using an IVIS 200 fluorescence reflectance imaging system (Xenogen Corp., Alameda, California). In order to account for autofluorescence, organs from SCID mice that had been injected with only PBS were also collected, homogenized and fluorescence measured. The autofluorescence of each organ homogenate was then subtracted from the experimental organ homogenates.

The presence of the phage particle's cpVIII within tissue homogenates was confirmed using immunoblotting. Tissue homogenates at a concentration of 5 mg/ml crude protein were electrophoresed on 16% Tricine gels and transferred to nitrocellulose membranes. cpVIII was detected by incubating the membrane with a rabbit polyclonal anti-cpVIII phage antibody at room temperature for 2 hours, and then extensively washing with TBS + 1% Tween. A goat anti-rabbit antibody conjugated to horseradish peroxidase was added and allowed to incubate at room temperature for 2 hours. The membrane was washed with TBS + 1% Tween and chemiluminescent peroxidase substrate (SuperSignal® West Pico, Pierce, Rockford, Illinois) was added then exposed to autorad film and developed.

Imaging of PC-3 xenografted tumors: Male SCID mice implanted with PC-3 cells as outlined above were chemically depilated over the lesions 24 hours prior to *in vivo* imaging in order to minimize autofluorescence and maximize signal. A fluorescence reflectance image was obtained prior to and after (immediate, 1, 4, and 24 hours) the intravenous injection of 10^9 IU of phage. Fluorescence reflectance imaging was performed using a bonSAI system (Siemens Medical, Germany) with the animals under gas anesthesia. Fluorescence signals were measured using ImageJ software (*48*) choosing

consistent exposure times. Tumors were resected for histo-pathology directly after the last timepoint.

RESULTS

A 15 amino acid fUSE5 phage display library (GenBank accession AF246445) was pre-cleared of phage clones that bound to organs and vasculature antigens in normal CF-1 mice, amplified, and used as the input phage for the *in vivo* selection of PC-3 prostate tumor binding phage. After four rounds of successive *in vivo* selection, 96 phage clones were sequenced and compared to our laboratory's phage-peptide sequence database (data not shown). When compared to our database, nineteen clones were found to be unique and were thus further pursued. Align, PIR, NiceBlast, gapped and PSI-BLAST search algorithms were used to analyze the foreign amino acid sequence inserts of the 19 clones, however no significant similarities to other proteins were found (*44, 45*). The 19 clones were analyzed for specificity using a two-tier micropanning procedure. In the first tier of the assay, phage were micropanned against PC-3 derived tumor tissue and normal muscle tissue. Nine phage clones generated a tumor to muscle specificity ratio of 1.5 or higher and were carried forward to be analyzed in the next stage of micropanning. The second tier of micropanning was used to select phage clones that bound preferentially to *in vitro* cultured PC-3 tumor cells. Of the nine phage clones carried forward from the first tier of micropanning, two (D9 and E8) did not bind at all to cultured PC-3 cells, six had a ratio less than 1.0 (D4, D7, F1, F6, F12, and G8), and only one (G1: IAGLATPGWSHWLAL) had a ratio greater than 2 (Table 1). The G1 phage produced a greater than 1.5 signal to noise ratio in the first tier of micropanning and

yielded the highest ratio in the second tier of micropanning, demonstrating specificity of binding to PC-3 derived tumors and *in vitro* cultured prostate carcinoma cells. Therefore, G1 (GenBank accession EF081458) was chosen for further characterization and given the name selected prostate carcinoma homing (SPCH) phage.

In order to directly detect phage and explore their use in cancer detection, SPCH and WT phage were labeled with AF680 at an average of ~600 AF680 molecules per phage particle. A modified ELISA was employed to investigate the effect of AF680 labeling on phage affinity for cultured PC-3 prostate carcinoma cells (Figure 2). The presence of AF680 on the surface of the phage lead to no significant change in the binding of SPCH or WT phage to cultured PC-3 prostate carcinoma cells. At phage concentrations between 5.0×10^{10} and 1.0×10^{11} virions/ml, SPCH phage exhibited a ~3 fold increase in binding to the PC-3 carcinoma cells compared to AF680 WT phage (Figure 2).

The binding patterns of the NIRF labeled phage were compared to those of free peptide to ensure that the binding properties of SPCH phage were due to the presence of the peptide and not to potential inherent non-specific binding of fd phage particles (*49, 50*). Laser scanning confocal microscopy was used to investigate and compare the binding of biotinylated free peptide and peptide displayed on AF680 labeled phage particles (Figure 3A). AF680 labeled SPCH phage and biotinylated, free SPCH peptide both displayed high intensity, cell membrane associated binding to cultured PC-3 cells and little to no binding to HEK 293 cells, demonstrating the specificity of the SPCH peptide to PC-3 cells. In contrast, AF680 labeled WT phage and biotinylated, free control peptide resulted in no significant binding to either cultured PC-3 or HEK 293

17

cells. Specificity of binding of AF680 labeled SPCH phage to other cultured cells was further investigated using confocal microscopy. It was found that AF680 SPCH phage bound to the prostate carcinoma cell lines PC-3, PC-3M (highly metastatic subline derived from PC-3), LNCaP (lymph node metastasis), and DU145 (derived from a brain metastasis) (Figure 3B). AF680 SPCH phage bound with highest intensity to PC-3 cells and slightly reduced intensity to the other human prostate carcinoma cell lines tested. Little to no binding of AF680 SPCH phage was observed to RPWE-1 (a normal human prostate cell line), MB-MDA-435 (a human breast carcinoma cell line), and HEK 293 cells. Micropanning data for these seven cell lines was consistent with these results (data not shown). These data demonstrate that binding of the SPCH phage is due to the presence of the SPCH peptide and that the peptide is specific for prostate carcinomas.

To determine the *in vivo* distribution of the SPCH phage clone, we injected AF680 labeled SPCH phage into SCID mice bearing subcutaneously implanted PC-3 cell derived tumors (Figure 4A). Both the AF680 SPCH phage and WT phage cleared through the organs of the reticuloendothelial system (RES), such as liver and lung as well as through the kidney (Figure 4A and B). AF680 phage began to amass in the RES as early as 5 minutes and continued at 6 hours. Muscle, fat, brain, and spleen exhibited very low levels of fluorescence. Accumulation of AF680 SPCH phage in the tumor began as early as 5 minutes and peaked from 4 to 6 hours. The tumor:fat uptake ratio for AF680 SPCH phage was ~10 at 4 hours post injection, in contrast to ~3 for AF680 WT phage. The tumor:muscle uptake ratio for AF680 SPCH phage was ~30 from between 30 minutes and 6 hours post injection. In contrast, the tumor:muscle uptake ratio for WT phage was ~11 at 5 minutes post injection and diminished to ~8 by 6 hours post injection. Notably,

the AF680 labeled SPCH phage yielded a 73% higher mean in tumor fluorescence over that of AF680 labeled WT phage at 4 hours post injection. These data provide evidence for binding of SPCH phage to xenografted PC-3 tumors in SCID mice.

The presence of phage particles in the tissue homogenates was verified by immunoblotting (Figure 5A). The immunoblots demonstrated the presence of phage in the liver as well as the tumor, confirming the biodistribution results and the fluorescent distribution of AF680 (Figure 5B). These findings support the results of the fluorescent biodistribution studies of AF680, and indicate that the intensity of AF680 fluorescent signal measured corresponds to the presence of phage in the tissues and organs. Furthermore, phage isolated from liver and tumor extracts by PEG precipitation were spectrophotometrically scanned from 600 nm to 800 nm (for AF680) and 240 to 320 nm (for phage particles), demonstrating that the fluorescence and phage particles co-precipitated (data not shown). Taken together, these data suggest that AF680 labeled SPCH phage are stable *in vivo*, and as such, could easily be utilized as an *in vivo* imaging agent.

To explore the usefulness of SPCH phage as an *in vivo* imaging agent we performed surface reflectance imaging with AF680 labeled SPCH phage. AF680 labeled phage could be imaged in the PC-3 derived tumors in SCID mice as early as 1 hour post injection (Figure 6). The peak of signal intensity and specificity within the tumor occurred at 4 hours post injection, which is consistent with the distribution data presented in Figure 4. At four hours post-injection of AF680 SPCH phage, a 4.5 fold increase in the fluorescent signal within the tumor compared to that of the normal tissue was observed with a specificity of 2.1 fold (SPCH to WT phage tumoral accumulation).

Together these data confirm that the SPCH peptide displayed on the tip of cpIII has a direct influence over the extravasation, accumulation, and retention of AF680 labeled phage within the tumor and that this sequence is specific for prostate tumors.

DISCUSSION

We selected *in vivo*, phage that target human PC-3 prostate carcinomas heterotransplanted in SCID mice. The phage clone SPCH displaying the peptide sequence IAGLATPGWSHWLAL, bound both cultured PC-3 carcinoma cells *in vitro*, and PC-3 tumors, *ex vivo*. More importantly, fluorescently labeled versions of the phage resulted in increased signal intensity within the PC-3 xenografted tumors in SCID mice. These results provide proof of principle that filamentous phage can indeed be used for the *in vivo* selection of extravasating phage that specifically target cancer cells which can be fluorescently labeled for use as a non-invasive tumor imaging tool.

Selection of extravasating phage that bound tumor cells was accomplished by first pre-clearing the 15 amino acid fUSE5 phage display library in normal mice, so as to remove unwanted phage that bound organs and normal vasculature components. The pre-selected library was incubated in the tumor bearing mice for times sufficient for extravasation to occur (*42*). From this *in vivo* selection, the peptide inserts of 96 phage clones were determined and compared to our laboratory's database of phage-displayed peptide sequences. Only 19 clones were unique to this particular phage display selection, supporting the notion that phage display procedures often result in "winning" clones that may be obtained due to inherent undesirable properties such as high infectivity, good growth capabilities, or hydrophobic non-specific binding properties (*50*). A two-tiered

20

micropanning assay was designed to identify which if any of the 19 clones had preferential affinity for both PC-3 prostate tumors and PC-3 cultured carcinoma cells. Because fd-phage often exhibit non-specific binding (*49, 50*), the first tier of micropanning was used as an indication of the level of background noise (binding of phage to normal tissue) as well as the ability of the phage to specifically bind tumor tissue. However, a positive finding in such an assay does not guarantee binding of the phage to the actual tumor cells, since tumor tissue is obviously composed of tumor cells in addition to connective tissue, extracellular matrix components, etc. The second tier of micropanning was then used as an indication of whether the selected phage bound to PC-3 cells themselves or could bind normal cells such as HEK 293 kidney cells. The ratio of binding of PC-3 cells to HEK 293 was calculated and only one clone (SPCH) had a ratio over 2, and was further investigated.

In vitro characterization of the AF680 SPCH phage binding properties, compared to that of AF680 WT, included both a modified ELISA and confocal microscopy. These assays provided proof of the AF680 labeled SPCH phage binding to cultured PC-3 cells *in vitro*. The SPCH sequence was not specific for PC-3 cells in that binding to other human prostate cancer cells was observed. Importantly, confocal microscopy indicated that SPCH phage bound with much higher affinity to cultured human prostate carcinoma cells than to RPWE-1 normal prostate, MB-MDA-435 breast carcinoma, or HEK 293 embryonic kidney cell lines. Thus, the SPCH sequence may target a prostate cancer-specific antigen. The very low background of AF680 WT phage observed in confocal microscopy (Figure 3A and B) was likely due to the fact that the cultured cells were pre-fixed with formaldehyde and, therefore, could be washed much more vigorously than the

live cells used for the micropanning and modified ELISA. Both *in vitro* assays with AF680 SPCH phage exhibited a $\geq$ 3 fold increase of signal from AF680 SPCH over that of AF680 WT.

In vivo characterization of the AF680 SPCH phage included biodistribution studies as well as optical imaging. Biodistribution of AF680 labeled SPCH and WT phage in PC-3 xenografted SCID mice exhibited similar distribution and clearance profiles. The muscle to tumor ratio found in the *in vivo* distribution was much higher than that found in the micropanning assay. This is most likely due to the inability of the large phage particles to extravasate *in vivo* into the muscle tissue, which maintains very tight junctions between endothelial cells.   In comparison, the micropanning assay involves incubation of a large concentration of phage within the homogenized tissue, thus allowing the characteristic non-specific binding of phage.   Another reason for the difference of muscle to tumor ratios found with micropanning versus *in vivo* biodistribution was the stringency of the micropanning assay.   The micropanning experiments utilized very stringent washing and detergent elution techniques. Additional micropanning experiments using a more traditional acid elution (*41*) generated a ratio of recovered phage from PC-3 versus HEK 293 of 5, compared to that of 2.14 from the more stringent CHAPS detergent elution.   Thus, the technique used within micropanning experiments has a direct impact on the number and type of phage recovered from the tissue or cell pellet. The high background binding found for WT phage in the *in vitro* assays is not unexpected, as phage are well known to bind to various supports such as plastic (*51*). Our goal was not to reduce the non-specific *in vitro* binding, but find phage that extravasated and targeted the tumor *in vivo*. The SPCH phage had a tumor/muscle

22

ratio of 30 *in vivo* suggesting that high backgrounds *in vitro* do not necessarily correlate with *in vivo* tumor targeting.

In review of the biodistribution data we observed clearance of the phage particles through the RES which is consistent with previous observations from our laboratory (*42*) as well as others (*13, 52*). It was found in the distribution studies that AF680 labeled SPCH phage accumulated and bound to human prostate PC-3 tumors *in vivo* with a 73% higher mean over that of AF680 labeled WT phage. The *in vivo* surface reflectance imaging with AF680 SPCH phage resulted in a 2 fold increase over background signal from AF680 labeled WT phage. Both of these findings are in agreement with the results from the *in vitro* assays.

SPCH phage and the corresponding peptide demonstrated preferential binding to human prostate carcinoma cell lines. In an effort to identify the targeted antigen, protein search algorithms were employed, however, no significant homologies to SPCH were found. This result is not surprising, in that only a handful of antigens targeted by *in vivo* selected peptides have been identified (*50, 53, 54*). The vast majority of peptides have targeted integrins via RGD-like or similar peptide motifs (*37, 54*). Furthermore, affinity chromatography experiments utilizing the SPCH sequence with extracts of cultured prostate cancer cell lines did not yield a candidate protein antigen (data not shown). Taken together, these results suggest the target of SPCH may be an inabundant protein antigen or a complex antigen consisting of protein, lipid, and/or carbohydrate components (*55*). Our findings further support the idea that *in vivo* selection of phage can be used to target rare and unique biomarkers on cancer cells, not merely vascular components.

The use of labeled phage as an alternative to labeled peptides for screening for tumor targeting agents has several advantages. First and foremost is affordability and speed, since synthesis and labeling of multiple peptides is a more costly and lengthy procedure. Screening of phage particles allows for more flexibility than screening of peptides. Initial screening of phage displaying selected peptides can be accomplished biologically by tracking the phage spectrophotometrically or by titering on host *E. coli*, whereas, peptides must be tagged. Addition of fluorophores, radiochelators, and epitope tags can have negative effects on the binding properties of the peptide (*11*). Hence, implementation of peptides displayed on phage may be a useful gauge of the ability of the synthesized peptide to bind its target before laborious peptide modifications ensue.

Because phage are organic and non-pathogenic (*13, 52*) they may be thought of as multifunctional, self replicating biological nanoparticles (*56*) in that they can be covalently attached to numerous tags or labels while simultaneously expressing multiple copies of foreign peptides. The resulting signal amplification is of enormous benefit to the peptide screening process and may expedite discovery and characterization of a "dark horse" peptide, without the documented side effects of other nanoparticles with metallic cores (such as cadmium-selenium or other metals) (*57-60*). Signal amplification is also beneficial to the characterization of phage displaying peptides in *in vivo* models of disease such as cancer. It allows for quick and easy characterization of the distribution profile of the peptide. As the phage have their own distinct *in vivo* distribution, the peptide bearing phage would need to be compared to a phage particle with no displayed peptide.

The study presented here describes the *in vivo* selection of phage specific to human prostate carcinoma. The ability of the resulting selected phage to be directly NIRF labeled and utilized for the *in vivo* imaging of human PC-3 prostate carcinoma highlights the simplicity and versatility of phage display technology.

Table 1: Two-step phage micropanning assay to evaluate specificity of selected

phage clones.

Newton JR, Kelly KA, Mahmood U, Weisleder R, and Deutscher SL (2006). In Vivo Selection of Phage for the Optical Imaging of PC-3 Human Prostate Carcinoma in Mice. *Neoplasia* 8(9); 772-780.

		First Round			Second Round		
Clone#	Sequence	Normal Tissue	Tumor Tissue	Ratio	HEK Cells	PC-3 Cells	Ratio
D4	GTRQGHTMRLGVSDG	21000	315000	15.00	108000	96000	0.89
D7	GDVWLFKTSTSHFAR	24000	300000	12.50	480000	66000	0.14
D9	LWVFPAGGHLGRERS	39000	270000	6.92	NT	NT	
E8	VMVPYSVRDSLFGSF	75000	156000	2.08	NT	NT	
F1	SVGGWFRQHLVGTRM	1200	6000	5.00	2400	1500	0.63
F6	LASIVRWEQVPDALS	12000	21000	1.75	5400	300	0.06
F12	SGVWAPTAGYDAGFH	13500	27000	2.00	7800	5100	0.65
G1	IAGLATPGWSHWLAL	10800	18000	1.67	8400	18000	2.14
G8	SHSDYRPAPWSGWML	600	2400	4.00	2700	2400	0.89

**Figure 2: Binding of AF680 labeled phage and unlabeled phage to PC-3 human prostate carcinoma cells**.

Newton JR, Kelly KA, Mahmood U, Weisleder R, and Deutscher SL (2006). In Vivo Selection of Phage for the Optical Imaging of PC-3 Human Prostate Carcinoma in Mice. *Neoplasia* 8(9); 772-780.
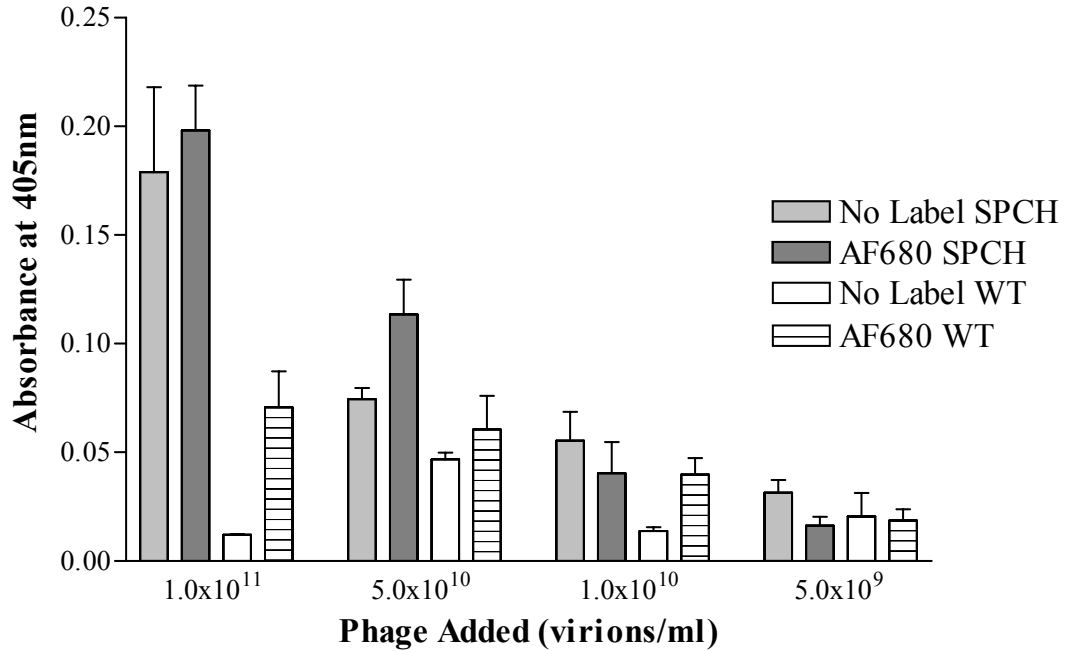
PC-3 human prostate carcinoma cells were grown to 90% confluency in a 96-well plate. $5x10^9$, $1x10^{10}$, $5x10^{10}$, or $1x10^{11}$ virions/ml of phage was added to the wells containing complete growth media and allowed to incubate for 1.5 hours at 37°C. Cells and attached phage were then washed with ice cold PBS and fixed with 4% formaldehyde. Presence of phage was detected by a rabbit polyclonal anti-phage antibody, followed by an anti-rabbit antibody conjugated to horseradish peroxidase. Liquid peroxidase substrate was added and the plate was then read on a μQuant Universal Microplate Spectrophotometer at an absorbance of 405nm.

Figure 3: Binding of AF680 labeled phage and peptide to human carcinoma cells and control normal cells.

Newton JR, Kelly KA, Mahmood U, Weisleder R, and Deutscher SL (2006). In Vivo Selection of Phage for the Optical Imaging of PC-3 Human Prostate Carcinoma in Mice. *Neoplasia* 8(9); 772-780.
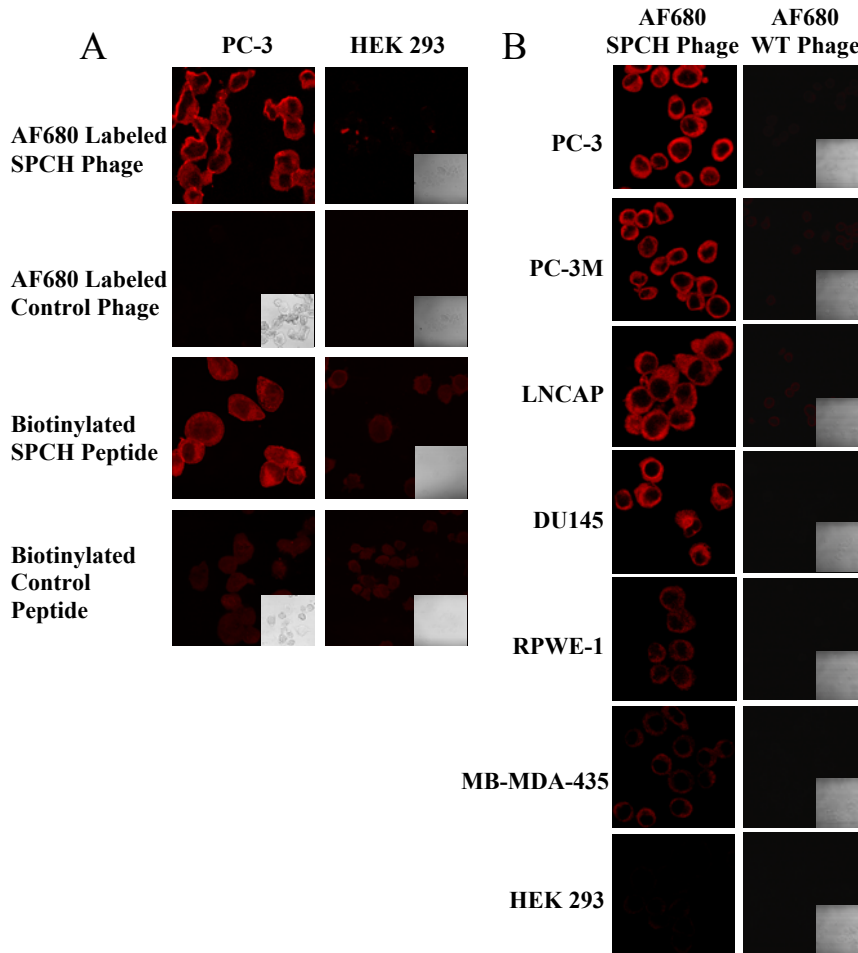
Slides containing fixed PC-3 or HEK 293 cells were incubated with AF680 labeled phage solutions (1×10^{11} virions/ml phage in 10 mM Tris, pH 7.5, 1% BSA) or biotinylated peptide solutions (20 μM peptide in 10 mM Tris, pH 7.5, 1% BSA) for 1 hour in the dark, at room temperature. Binding of biotinylated peptide was detected by using 10 μg/ml NeutrAvidin-Texas Red (Figure 3A). Specificity of binding was determined by incubating AF680 SPCH or WT phage on slides containing PC-3, PC-3M, LNCaP,

DU145, RPWE-1, MB-MDA-435, and HEK 293 cells (Figure 3B). Presence of fluorophore was detected by laser scanning confocal microscopy.

Figure 4: Biodistribution of AF680 labeled SPCH fUSE5 and WT phage in PC-3 xenografted SCID mice.

Newton JR, Kelly KA, Mahmood U, Weisleder R, and Deutscher SL (2006). In Vivo Selection of Phage for the Optical Imaging of PC-3 Human Prostate Carcinoma in Mice. *Neoplasia* 8(9); 772-780.
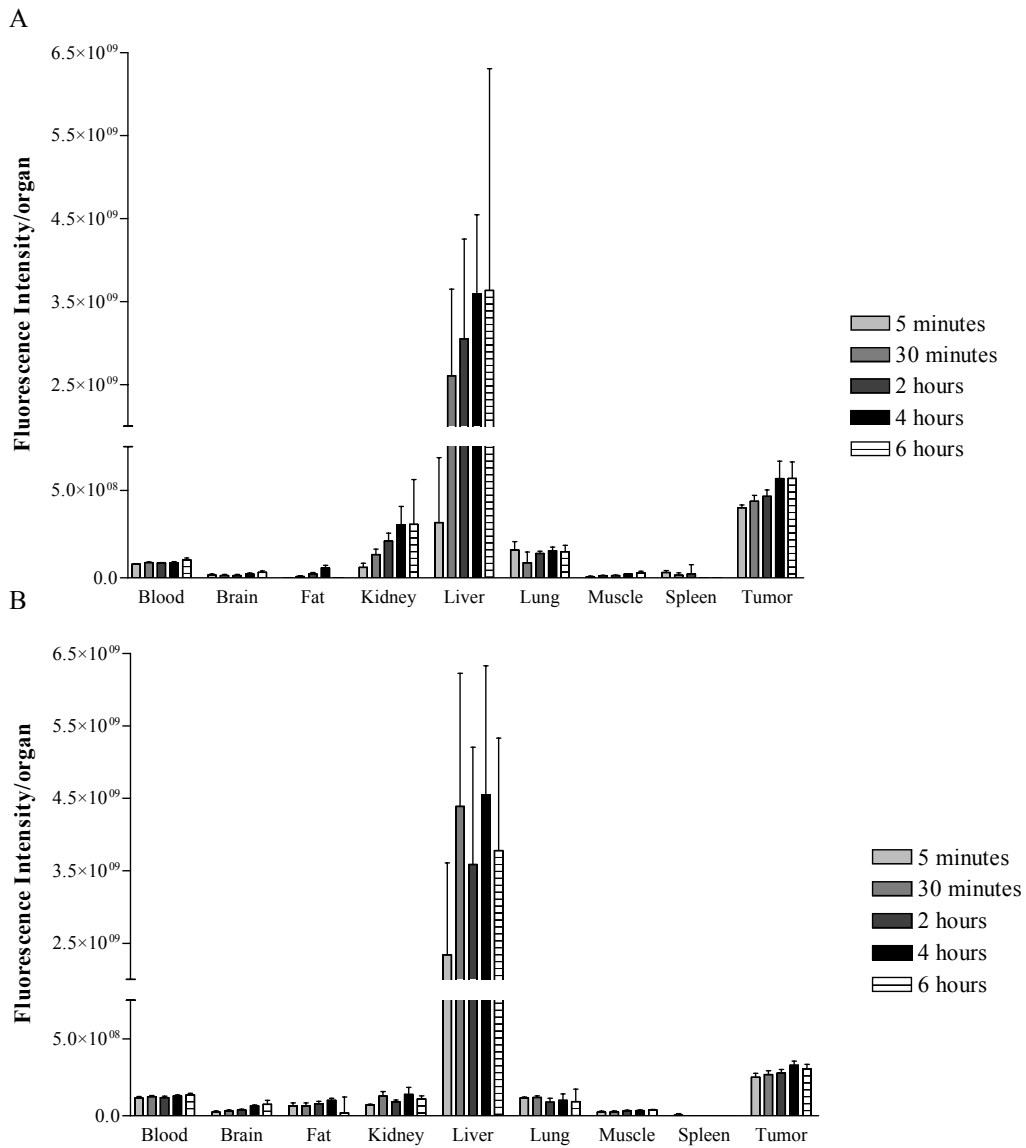
SCID mice bearing human PC-3 carcinoma tumors were injected with ~10^9 IU of AF680 labeled SPCH fUSE5 phage (Figure 4A) and AF680 labeled WT phage (Figure 4B) and were allowed to circulate for 5 minutes, 30 minutes, 2 hours, 4 hours and 6 hours. Organs were excised, homogenized, and probed for fluorescent activity using the Xenogen IVIS 200 system.

Figure 5: Biodistribution of AF680 labeled SPCH fUSE5 and WT phage in PC-3 xenografted SCID mice.
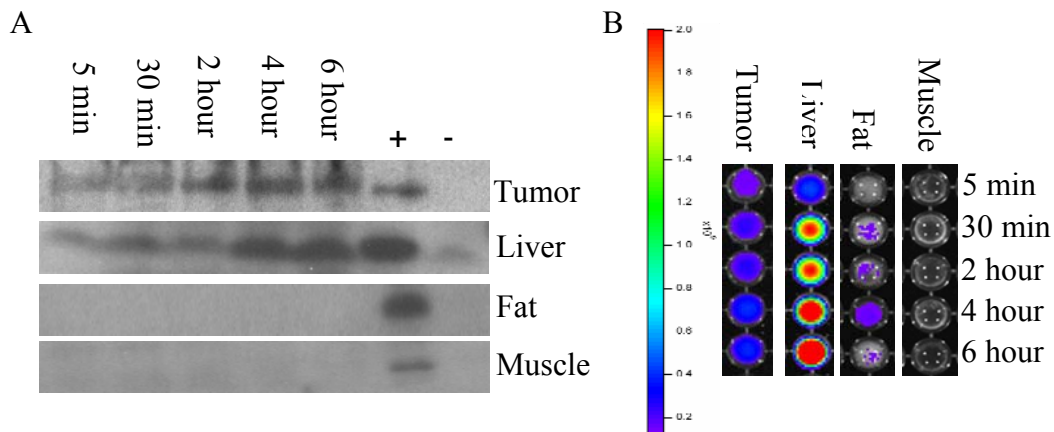
Newton JR, Kelly KA, Mahmood U, Weisleder R, and Deutscher SL (2006). In Vivo Selection of Phage for the Optical Imaging of PC-3 Human Prostate Carcinoma in Mice. *Neoplasia* 8(9); 772-780.

Homogenized tissues from SCID mice bearing human PC-3 carcinoma tumors were probed for fluorescent activity of the AF680 label and for the presence of cpVIII. The presence of the phage cpVIII was verified by immunoblotting of tumor, liver, fat and muscle (Figure 5A). Homogenized tissues were electrophoresed on 16% Tricine gels and transferred to 0.45 μm nitrocellulose membranes. cpVIII was detected by incubating the membrane with a rabbit polyclonal anti-cpVIII phage antibody followed by a goat anti-rabbit antibody conjugated to horseradish peroxidase. Signal was determined by addition

of chemiluminescent peroxidase substrate, exposure to double emulsion Blue Lite autorad film and development of the film using Kodak Processing Chemicals. Homogenized tumor, liver, fat, and muscle were probed for fluorescent activity using the Xenogen IVIS 200 system (Figure 5B).

Figure 6: *In vivo* imaging of a PC-3 prostate tumor using AF680 labeled SPCH fUSE5 phage.

Newton JR, Kelly KA, Mahmood U, Weisleder R, and Deutscher SL (2006). In Vivo Selection of Phage for the Optical Imaging of PC-3 Human Prostate Carcinoma in Mice. *Neoplasia* 8(9); 772-780.
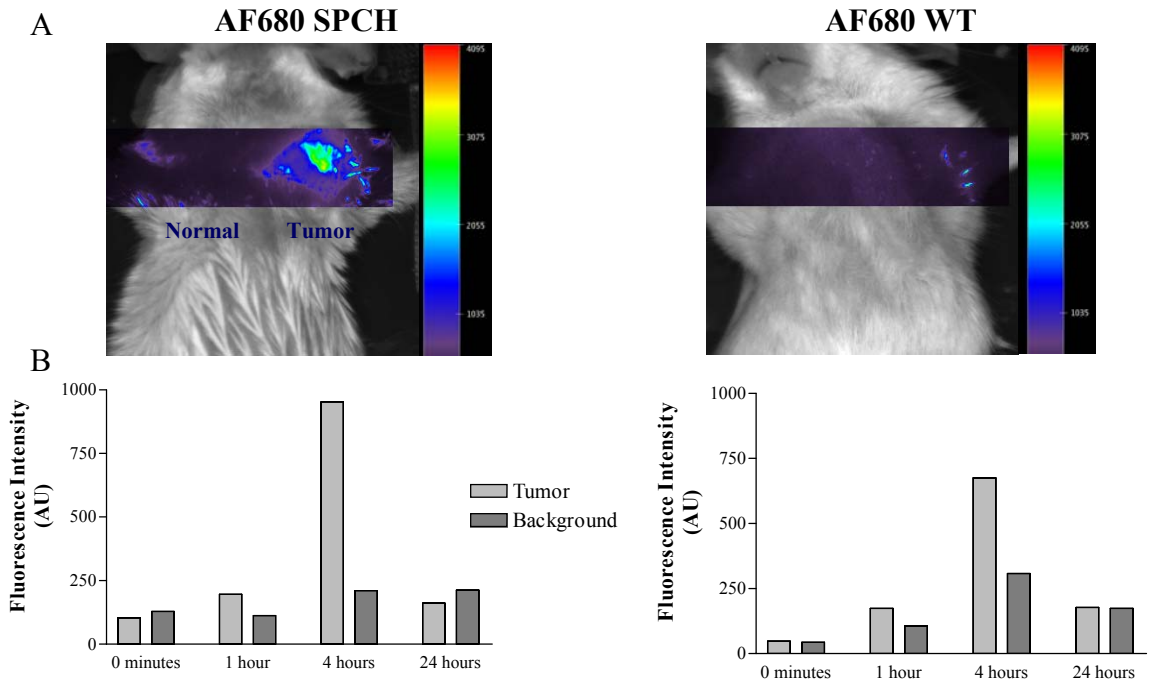
SCID mice bearing PC-3 tumors were injected with AF680 labeled SPCH or WT phage. Images were taken at 0 minutes, 1 hour, 4 hours and 24 hours post injection.

CHAPTER 3

TWO-STEP RADIOIMAGING

INTRODUCTION

Bacteriophage (phage) display is a well established combinatorial chemistry technique that employs a population of fd filamentous phage genetically modified to display a library of random peptides on their surface (*38*). One such library commonly used is the fd-tet fUSE5 library. This library contains phage with a modified coat protein III displaying up to five copies of a fused random peptide on the tip of the phage particle. Affinity selection of phage constructs is preformed via multiple rounds of stringent washing and amplification (*38*). Traditionally, the selected targeting peptide(s) are synthesized and their *in vitro* and *in vivo* binding is then characterized (*38, 61, 62*). Phage display has proven itself useful in the identification of novel binding ligands for proteins, carbohydrates, and nucleic acids (*32, 33, 36, 63, 64*).

Recently, phage display has been used for the discovery of new and unique cancer imaging peptides (*34, 65, 66*). Of these tumor homing peptides, only a handful have been developed into non-invasive cancer imaging agents (*53, 67*). One reason for this may be due to differences in peptides fused to phage coat proteins versus chemically synthesized peptides (*65, 68*). The conformational structures of the selected, fused peptides are impacted by the microenvironment created by the surface of the phage particle. Thus, synthetic peptides, derived from sequences selected on the phage, can have binding characteristics that contrast from those of the peptides displayed on the surface of the phage particle. Another disadvantage to the use of the synthesized selected peptides for

the imaging of cancer is the covalent addition of radiochelators and/or fluorescent tags to a small peptide can often have deleterious effects on the peptide's binding affinity for its target (*11*). Conversely, covalent addition of imaging tags to a phage particle has minimal effect on the displayed peptide's ability to bind its target (*69*). It would therefore be advantageous to use labeled phage for the validation of a selected peptide's tumor targeting propensity.

Direct imaging with very large molecular weight phage particles presents its own set of challenges. Previous studies of the distribution and clearance profiles of fd filamentous phage in mice (*13, 70*) demonstrated clearance of phage through the reticuloendothelial system and, therefore, accumulation of large amounts of phage in the liver, spleen, and lung was observed. Phage, intravenously injected into a mouse, take ~48 hours to completely clear from the tissues; though they have an average blood half life of ~15 minutes (*70*). Implementation of a two-step pretargeting system could allow for the clearance of the majority of the phage before injection of the imaging label. We propose that the use of biotinylated phage displaying tumor homing peptides in combination with radiolabeled streptavidin (SA) may offer a novel approach to imaging cancer in animals.

Here we employed a well described, high affinity peptide-receptor system, namely the melanocortin-1 receptor (MC1 receptor) and its ligand the peptide alpha-melanocyte stimulating hormone (α-MSH) (*71, 72*), for the development of a phage-based pretargeting strategy for melanoma imaging. MC1 receptor possesses a nanomolar affinity for its ligand and has been found to be overexpressed on up to 80% of human melanomas from patients with metastatic lesions (*73*). Alpha-MSH peptide analogs were

33

engineered and fused with the phage coat protein III using the fUSE5 vector to employ them as melanoma imaging agents. Biotinylated fUSE5 phage displaying the α-MSH peptide analog (bio-MSH2.0 phage) were able to target the cell surface receptor, MC1 receptor (*72*), on B16-F1 mouse melanoma cells both *in vitro* and *in vivo*. Analysis of *in vivo* distribution data revealed selective tumor uptake and retention within syngeneic grafted B16-F1 melanoma tumors of C57/BL6 mice over a 24 hour time period (post injection of ^{111}In-radiolabeled streptavidin (^{111}In-SA)). Imaging studies revealed that intravenously injected biotinylated MSH phage resulted in tumor targeting four hours post injection of ^{111}In-SA. These studies provide proof of principle that phage display technology coupled with a pretargeting approach could offer a powerful and efficient means to enhance the discovery of novel imaging peptides and assess their tumor-targeting propensities *in vivo*.

MATERIALS AND METHODS

Materials: Cell culture reagents were purchased from Invitrogen (Carlsbad, CA). All other chemicals were purchased from Sigma Chemical Company (St. Louis, MO), unless otherwise stated.

Cell lines: B16-F1 mouse melanoma cells (American Tissue Culture Collection, Manassas, VA) were grown in complete media (RPMI 1640 media, 10% fetal bovine serum, 2 mM L-glutamine, and 48 μg/ml gentamicin) at 37°C in 5% CO_2. The cell line was tested for pathogens before injection into mice.

Generation of clonal phage populations: Clonal phage populations of the α-MSH peptide analogs, MSH1.0 (ASYSMEHFRWGRPVAG) or MSH2.0 (GenBank

accession EF081459) (AMEHFRWGRPVGSGSGSGSVWYAG), were generated using the fUSE5 vector (generous gift from George Smith) as previously described (*41*). Briefly, fUSE5 vector was digested with the *Sfi*I restriction endonuclease. Equal molar amounts of sense and antisense phosphorylated DNA oligonucleotides were hybridized in STE buffer (50 mM NaCl, 10 mM tris, pH 8.0, and 1 mM EDTA) by heating to 94ºC and slowly cooling to room temperature. A room temperature DNA ligation reaction was preformed for the insertion of the hybridized DNA into the fUSE5 vector. *Escherichia coli* (*E. coli*) K91 Blue Kan cells were electroporated in the presence of the ligated vector, amplified in 2 ml NZY broth with 20 µg/ml tetracycline. Proper DNA sequence was verified by DNA sequencing using the University of Missouri DNA core facility. Infected cultures were expanded to 1 liter and the amplified phage were polyethylene glycol (PEG) precipitated. The PEG-precipitated phage were further purified by cesium chloride ultracentrifugation. Following dialysis in 1X Dulbecco's PBS, Ca^{2+} and Mg^{2+} free (PBS), the phage particle concentration in virions (V) was determined spectrophotometrically. *E. coli* K91 Blue Kan (a host strain for filamentous phage) was used in a titration assay to quantitate the concentration of infectious units (infectious units, IU) within the purified sample. The resulting titer of phage is expressed in terms of IU/ml.

Phage dot blots: Two sequential 1 µl dots of 1 x 10^{11} V/ml phage solution of MSH1.0, MSH2.0, and wild-type (*47*) were allowed to air dry on a 0.2 µm nitrocellulose membrane followed by blocking overnight at 4ºC with 6% BSA in Tris buffered saline, pH 7.0 (TBS). The presence of phage particles was detected by addition of rabbit polyclonal anti-phage antibody (courtesy of George Smith) at a dilution of 1:1000. The

primary antibody was incubated with the membrane at room temperature for 1 hour followed by extensive washing with TBS+1% Tween-20. An anti-rabbit antibody conjugated to horseradish peroxidase (Santa Cruz Biotechnology, Santa Cruz, CA) was then added at a 1:1500 dilution and allowed to incubate with the membrane at room temperature for 1 hour. The membrane was washed with TBS+1% Tween-20, rinsed with dH$_2$O, and immersed in 4CN peroxidase substrate solution (KPL, Gaithersburg, MD). This same procedure was followed for the detection of the C-terminus of α-MSH using a sheep anti-C-terminal α-MSH antibody (Chemicon, Temecula, CA) and anti-sheep conjugated to horseradish peroxidase (Santa Cruz Biotechnology, Santa Cruz, CA).

Micropanning of biotinylated and non-biotinylated phage: B16-F1 melanoma cells were grown to 80% confluency in 35 mm tissue culture treated plates (Fisher Scientific, Pittsburgh, PA) and removed using 1X PBS + 2mM EDTA. The suspension of cells was incubated in complete media with 10^8, 10^7 or 10^6 IU/ml of MSH 2.0 or WT biotinylated or non-biotinylated phage (input phage) for 1.5 hours at 37°C. The cells were then washed five times with PBS. The final cell suspension containing 2.5% CHAPS, was then titered on *E. coli* K91 Blue Kan (recovered phage).

Biotinylation of phage: NHS-PEO$_4$-biotin (Pierce Biotechnology, Rockford, IL; MW 588.67 daltons) was dissolved in DMSO and added to a suspension of phage in 100 mM NaH$_2$PO$_4$ (pH 7.4 with NaOH) at a 1000-fold molar excess over the phage particles, and rotated at room temperature for 2 hours. The reaction was stopped with a final concentration of 400 mM ethanolamine (pH 9.0) with rotation at room temperature for 1 hour. The phage preparation was then extensively dialyzed against TBS to remove excess free biotin.

Covalent attachment of DTPA to SA: *p*-SCN-Bn-DTPA (2-(4-isothiocyanatobenzyl)-diethylenetriaminepentaacetic acid) (Macrocyclics, Dallas, TX) was dissolved in carbonate buffer (0.5M sodium carbonate, pH 9.5) and added to SA suspended in 1X PBS yielding a mixture containing 50 fold more DTPA than SA. The mixture was rotated overnight at 4ºC. Excess DTPA was removed with Zeba Desalt Spin Columns (Pierce Biotechnology, Rockford, IL).

^{111}In-DTPA-SA stability: DTPA-SA was radiolabeled with ^{111}In by the addition of 0.37 MBq to 0.1 µg DTPA-SA in 10 mM HEPES (pH 7.0) followed by incubation at 37ºC for 1.5 hours. Excess ^{111}In was removed with Zeba Desalt Spin Columns (Pierce Biotechnology, Rockford, IL). The resulting purified sample was aliquoted into one of three different buffers: HEPES (10 mM, pH 7.0), 1X PBS, or normal mouse serum and incubated either at 25ºC or at 37ºC for 1, 4, 8, or 24 hours. Zeba Desalt Spin Columns were used to remove free ^{111}In and the resultant amount of radioactivity in the final and purified aliquots were then compared.

Biodistribution and SPECT/CT imaging of biotinylated phage and ^{111}In-DTPA-SA: All animal studies were conducted in accordance to the NIH guide for Care and Use of Laboratory Animals and the Policy and Procedures for Animal Research at the Harry S. Truman Memorial Veterans' Hospital. C57/BL6 mice were obtained from Harlan (Indianapolis, IN). The animals were provided with water ad libitum and fed biotin free rodent chow for 5 days prior to injection. C57/BL6 mice receiving 1x 10^6 B16-F1 murine melanoma cells were subcutaneously inoculated in the right flank or intrascapulary region. Ten days post-inoculation tumors weighed approximately 0.05 to 0.1 grams. Groups of 3 mice received tail vein injections of 5 x 10^{12} virions of

biotinylated phage. Phage were allowed to circulate for four hours (*47*) followed by another tail vein injection of 1.85 MBq of ^{111}In-SA. Mice were sacrificed by cervical dislocation at 0.5, 2, 4, 6, or 24 hours post injection for the purpose of harvesting the organs of interest. Each organ was weighed and counted in a Wallac 1480 automated gamma counter (Perkin Elmer, Wellesley, MA). Five mice were used for competition studies. These mice received tail vein injections of 5 x 10^{12} virions of bio-MSH2.0 phage mixed with 100 µg NDP, followed four hours later by injection of 1.85 MBq of ^{111}In-SA. Mice used for the purpose of imaging received a tail vein injection of 5 x 10^{12} virions of biotinylated phage followed by an injection of 7.40 MBq of ^{111}In-SA. The mice were euthanized four hours post injection of the radiolabel with carbon dioxide. Imaging was preformed by the USVA Biomolecular Imaging Center in the Harry S. Truman VA Medical Center using a micro-SPECT/CT System (Siemens Preclinical Solutions, Malvern, PA) equipped with high resolution 2 mm pinhole collimator. At the time of the SPECT scan there was approximately 2.81 MBq of ^{111}In-SA remaining in the mouse. A total of 1,349,826 counts were acquired by the SPECT image. The 78×78×102 volumetric isotropic voxel matrix data was reconstructed using a 3D-OSEM algorithm. This instrument was also equipped with an 80 k Vp x-ray source and software for 360º CT data acquisition. A fanbeam (Feldkamp) filtered back projection micro-CT image reconstruction algorithm was used for the production of a 512×512×960 isotropic voxel image matrix. Co-registered SPECT and CT data was visualized using Amira 3.1 (TGS, San Diego, CA).

RESULTS

The MC1 receptor - α-MSH receptor ligand system was employed to develop and characterize a new phage-based pretargeting strategy for melanoma imaging employing biotinylated phage and ^{111}In-SA. Phage displaying α-MSH peptide analogs were generated using the fUSE5 phage display vector (Table 1). These phage were then sequenced to confirm that the coding inserts were within the proper reading frame. The MSH1.0 phage clone was designed to display the native α-MSH peptide sequence displayed at the N-terminus of the phage coat protein III, while the phage clone MSH2.0 contained a modified MSH sequence. MSH2.0 lacked 3 non-essential amino acids at the amino terminus of the α-MSH sequence and contained a linker peptide between it and the phage coat protein III. The phage clones were probed with an anti-α-MSH antibody to determine if the peptide sequences were accessible and reactive with an antibody that recognizes the core receptor binding residues for the MC1 receptor. A phage particle dot blot was performed using the anti-α-MSH peptide antibody (Figure 7A). Results from the phage immunoassay revealed that the native α-MSH sequence displayed on phage clone MSH1.0 was not immunoreactive while MSH2.0 was recognized by the antibody. These results demonstrated that the α-MSH sequence on the MSH2.0 phage clone had greater reactivity and predicted more biological activity than the peptide on MSH1.0 phage.

A micropanning assay was utilized to test the specific binding of MSH2.0 phage (Figure 7B). After incubation of differing amounts of phage with B16-F1 cells, the washed and lysed cells were titered using *E. coli* K91 Blue Kan cells in order to quantify the amount of phage still bound to or internalized by the cells. Micropanning MSH2.0

phage against the mouse melanoma cell line B16-F1 with an input of 10^8 IU/ml phage, after extensive washing, resulted in an 18 fold higher recovery of MSH2.0 phage than that of WT phage. The WT non-specific background dropped to 200 fold below that of MSH2.0 with 10^7 IU/ml input phage. When 10^6 IU/ml input phage were incubated with the B16-F1 cells, no WT phage were recoverable. These results indicate the selective binding of phage displaying the peptide MSH2.0 to B16-F1 melanoma cells.

The MSH2.0 and WT phage were biotinylated with NHS-biotin as part of the biotin/SA pretargeting strategy. The biotin linker employed contained an extended, hydrophilic polyethylene oxide (PEO_4) spacer arm that may minimize possible steric hindrances involved with SA binding to biotin molecules on the surface of the large phage particle. Biotin on the surface of the virion was verified by inhibiting phage infection of *E. coli* in the presence of 0.05 μg/ml of SA (data not shown).

To determine if biotinylation of the MSH2.0 phage affected MC1 receptor binding, the micropanning assay was repeated with biotinylated phage constructs (Figure 7B). Figure 7B shows that the micropanning results of bio-MSH2.0 and bio-WT phage against B16-F1 cultured mouse melanoma cells mirrored the findings with the non-biotinylated phage. These results demonstrated that the addition of PEO_4-biotin to the surface of the phage particle resulted in no significant alteration of phage binding to cultured B16-F1 mouse melanoma cells *in vitro*.

SA, the second component of the two-step targeting system, was conjugated with the metal chelator DTPA through an isothiocyanate linkage. DTPA-SA complex exhibited greater than 90% labeling efficiency. Stability of the ^{111}In-SA compound was investigated in order to ensure the feasibility of extended *in vivo* use. ^{111}In-SA was

incubated in three different solutions, PBS, 10 mM HEPES, and mouse serum, and at two different temperatures, 25ºC and 37ºC (data not shown). After 24 hours samples incubated in mouse serum maintained ~80% of their original activity, while all other samples exhibited no statistically significant change in their retained activity. Thus, the ^{111}In-SA complex was sufficiently stable for *in vivo* applications.

The biodistribution and tumor targeting properties of pretargeted bio-MSH2.0 phage followed by ^{111}In-SA was investigated *in vivo* in the B16-F1 mouse melanoma model. Bio-MSH2.0 phage were injected into C57/BL6 mice with syngeneic grafted B16-F1 melanoma tumors and allowed to circulate for four hours. At predetermined time points post injection of ^{111}In-SA, mice were sacrificed and their organs and tissues were counted to determine the distribution of the radioactivity. Clearance of the ^{111}In radioactivity was found to be primarily through the urinary and hepatobiliary systems (Figure 8A). Tumor uptake of ^{111}In-SA appeared, initially, to be due to blood volume within the tumor. However, at 24 hours post injection, retention of ^{111}In-SA within the tumor was clearly observed with a value of 1.0±0.1 %ID/g (Figure 8A) and a tumor to blood ratio of 2.0±0.2 (Figure 8B).

To validate that the radioactivity found within the tumor at 24 hours post-injection was due to binding and retention of the bio-MSH2.0 phage the distribution of bio-WT phage followed by ^{111}In-SA was examined. The *in vivo* distribution of ^{111}In-SA alone was also examined. Tumor uptake at 24 hours post injection was found to be 0.4±0.1 %ID/g, while whole body clearance was found to be similar to previously reported results (*74*). Examination of tumor to muscle ratios for the different phage constructs revealed a preferential localization of ^{111}In-SA within the B16-F1 tumor due to the presence of bio-

MSH2.0 phage. The tumor to muscle ratio for bio-MSH2.0 phage was 17.5±3.7 at 24 hours post-injection (Figure 8B). In comparison, the tumor to muscle ratio for bio-WT phage was 3.0±0.6 at 24 hours post-injection (p=0.001). The accumulation of radioactivity within the tumor at 24 hour post-injection was 1.8±0.2 times greater in the mice injected with bio-MSH2.0 phage than those injected with bio-WT phage (p=0.003) (Figure 8C). These data suggest the targeting of bio-MSH2.0 phage to B16-F1 tumors *in vivo* is α-MSH peptide mediated.

To validate that the radioactivity found within the tumor was due to the specific binding of the bio-MSH2.0 phage, non-radioactive NDP peptide was co-injected with the bio-MSH2.0 phage (Figure 8D). NDP is a potent, protease resistant peptide analog of α-MSH commonly used in competition assays (*75*). The presence of the NDP peptide reduced ^{111}In-SA /bio-MSH2.0 phage retention by 2.4±0.4 fold (p=.002), demonstrating specificity of binding for bio-MSH2.0 phage *in vivo*.

The two-step phage pretargeting approach was employed for the *in vivo* imaging of solid mouse melanoma tumors. C57/BL6 mice bearing B16-F1 melanomas were imaged at 4 hours post injection of ^{111}In-SA using micro-SPECT/CT. SPECT imaging of the mice clearly demonstrated accumulation of the ^{111}In-SA, and thus the biotinylated phage displaying MSH2.0, within the tumor. SPECT/CT images representative of the melanoma bearing mice injected with bio-MSH2.0 phage are shown in figure 9. These results strongly suggest the use of biotinylated phage displaying tumor homing peptides combined with the use of radiolabeled SA in a two-step imaging process is a valuable approach for the validation of a selected peptide's ability to target and image tumors.

DISCUSSION

Two multivalent, bifunctional phage constructs, MSH1.0 and MSH2.0, were developed for the *in vivo* imaging of solid B16-F1 mouse melanoma tumors. MSH1.0, the native α-MSH peptide sequence (Table 1), was not immunoreactive possibly due to steric hindrance and/or conformational changes induced by the direct fusion with coat protein III (Figure 7A). In MSH2.0, the first three amino acids of the native MSH sequence were removed in an effort to place the conserved receptor binding sequences closer to the amino terminus where they may be more readily accessible. A spacer of four gly/ser amino acid repeats and a val-trp-tyr tri-peptide were then added to the carboxy terminus of the MSH2.0 sequence to protect the configuration of the peptide from any influence of secondary structures from coat protein III. MSH2.0 was found to be immunoreactive and both biotinylated and non-biotinylated MSH2.0 phage constructs were recognized and bound by the appropriate receptor, MC1 receptor, *in vitro*. Surprisingly, the ability to locate a functioning MSH targeting sequence on the phage particle was not as straightforward as expected. Directly fusing the targeting sequence to coat protein III appeared to alter the peptide conformation and limit ligand recognition. A spacer sequence had to be added between the MSH peptide and the coat protein to allow the targeting sequence to adopt a bioactive conformation. Had the α-MSH peptide sequence undergone a phage display-based affinity maturation, the optimal active conformation of the peptide on the phage coat protein would have been accounted for in the affinity selection process.

Alpha-MSH peptide sequences bind their cognate MC1 receptor with high affinity and specificity. Numerous MSH analogs have been chemically synthesized, radiolabeled

43

and examined for melanoma imaging and therapy. In comparison with pretargeted phage, ^{99m}Tc-radiolabeled linear MSH peptide analogs displayed higher tumor uptake values at early time points, but similar tumor uptake values at 4 hours post injection in B16-F1 melanoma bearing mice (76). Tumor uptake of ^{99m}Tc radiolabeled CGC-NDP and MAG$_2$-NDP at 4 hours were 0.56±0.14 and 0.74±0.15 %ID/g as compared to 0.9±0.4 for the pre-target MSH phage particle. Linear MSH peptide-DOTA conjugates displayed tumor uptake values ranging from 0.65±0.05 to 7.77±0.35 at 4 hours post injection and 0.23±0.01 to 2.32±0.15 at 24 hours (77), while pre-targeted phage exhibited 0.9±0.4 and 1.0±0.1 at 4 hours and 24 hours post injection. Pre-targeted MSH phage exhibited tumor-targeting properties similar to ^{99m}Tc-labeled linear-MSH peptide analogs and less than the optimal radiolabeled DOTA-conjugated peptides. Additional peptide structural engineering is likely to be required to achieve tumor uptake values of 10-20 %ID/g, which have been reported for metal cyclized MSH analogs (78, 79).

Upon analysis of the *in vivo* distribution of ^{111}In-SA it was evident that the clearance of the activity through the urinary track lead to kidney uptake and retention. The kidney retention of ^{111}In-SA even at 24 hours post injection was expected (Figure 8A). It is known that SA is a proteolytically stable protein and that the retention of SA within the kidney is largely due to its resistance to degradation (80). However, the observed kidney uptake of about 5 %ID/g is lower than many of the reported values within the literature (74, 80-82). This is likely a result of the lysine residues within the SA being altered after covalent attachment of the DTPA chelator. Previous work has shown that arginine and lysine residues within the SA protein contribute to the

accumulation of SA in the kidney (*74*). Modification of the lysine residues shifts the biodistribution of SA so that accumulation of SA is also seen in the liver and spleen (*81*).

Comparison of the *in vivo* distribution of ^{111}In-SA for mice injected with either bio-MSH2.0 phage or bio-WT phage revealed no change in the clearance of the radiolabel. However, tumor accumulation of the radiolabel was 1.8 fold more with bio-MSH2.0 phage compared to bio-WT phage (Figure 8C) and 2.7 fold more than ^{111}In-SA alone. Furthermore, there was a noteworthy difference in the tumor to muscle ratios of 17.5 and 3.0 for bio-MSH2.0 and bio-WT phage 24 h post injection, respectively (Figure 8B). The *in vivo* targeting specificity of MSH phage for the MC1 receptor was examined in an *in vivo* competitive binding study with the high affinity MSH peptide analog NDP (Figure 8D). The competitive binding study was performed at two hours post injection due to the pharmacokinetics of the NDP blocking peptide (*78*). Finally, SPECT/CT imaging of B16-F1 tumor bearing mice confirmed accumulation of the radiolabel within the tumor. These mice also had activity within the kidneys and intestines which is reflective of the distribution data that exhibited clearance of activity through the urinary and hepatobiliary systems. Further analysis of the mice used for imaging revealed a higher uptake of ^{111}In-SA/bio-MSH2.0 phage within the tumor at 5.2 ± 0.8 %ID/g compared to 0.9 ± 0.3 in the biodistribution studies. Increased tumoral accumulation was probably due to the larger dose of ^{111}In-SA administered. These data provided the proof necessary to demonstrate that the combination of phage display technology and pretargeting strategy allows for assessment of a peptide's *in vivo* tumor targeting ability. This newly described technique will prove useful for the *in vivo* screening of newly discovered phage display selected tumor targeting peptides.

It is envisioned that a pretargeting strategy can be employed to rapidly assess the tissue targeting properties of novel peptide sequences discovered via phage display selection *in vivo*. The MSH phage described in this report were developed as a proof of principle model for pretargeted phage imaging using a well characterized biological system. The strength of the pretarget approach is to support the efficient discovery of novel peptide imaging agents. There is an important need to expand the repertoire of peptides that bind novel cellular targets. Currently, there are a few peptide based imaging agents in the clinic (*83*) and numerous radiolabeled peptides undergoing pre-clinical research, but they bind only a hand full of unique cellular targets (*11*). Phage display technology is a powerful tool for the discovery of peptide ligands for novel molecular targets and pretargeted phage imaging will positively impact its efficiency and success. This study demonstrates the ability of pretargeted bio-MSH2.0 phage to target and image melanomas *in vivo*. This approach provides a simple, cost effective, and flexible imaging strategy useful for various applications including *in vivo* characterization of peptides and their tumor targeting propensities.

Table 2: Amino acid sequence of the native α-MSH sequence and MSH sequences displayed on the phage particles

Peptide	Sequence
α-MSH	NH_2- SYSMEHFRWGRPV
MSH1.0	NH_2-*ASYSMEHFRWGRPVAG-Coat Protein III
MSH2.0	NH_2-*AMEHFRWGRPVGSGSGSGSVWYAG-Coat Protein III

*Phage displayed α-MSH peptide analogs are flanked with an alanine residue, leftover from the cleavage of the signal peptidase, and coat protein III.

Figure 7: Binding of phage displaying α-MSH peptide analogs.
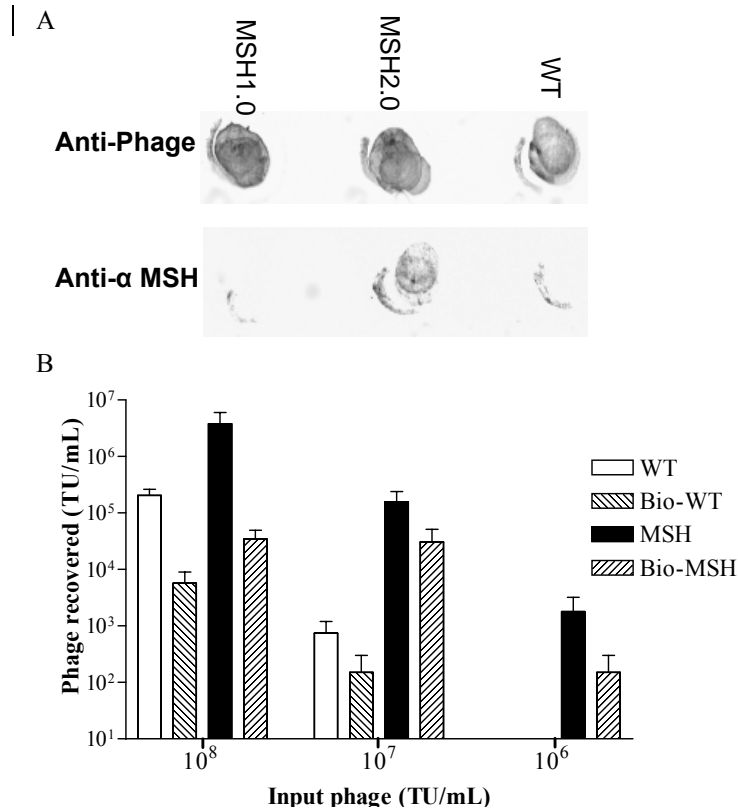
The presentation of the displayed α-MSH peptide analogs was probed by the ability of an anti-C terminus α-MSH peptide antibody to recognize and bind to the phage displayed peptide (A). Two 1 μl dots of 1×10^{11} V/ml phage solution were immobilized on nitrocellulose and the presence of phage particles was demonstrated using an anti-phage antibody. Presence of recognizable α-MSH peptide was determined using an anti-C terminus α-MSH peptide antibody. Complexes were detected using secondary antibody conjugated to horseradish peroxidase. The ability of the displayed peptide to be recognized and bound by the MC1 receptor on cultured B16-F1 melanoma cells was determined by micropanning (B). A suspension of B16-F1 melanoma cells was incubated with 10^8, 10^7 or 10^6 IU/ml of biotinylated or non-biotinylated phage for 1.5

hours, on a rotator, at 37°C. The cells were then extensively washed with PBS, and the

final wash containing 2.5% CHAPS was titered with *E. coli.*

Figure 8: Biodistribution of biotinylated phage and ^{111}In-SA.
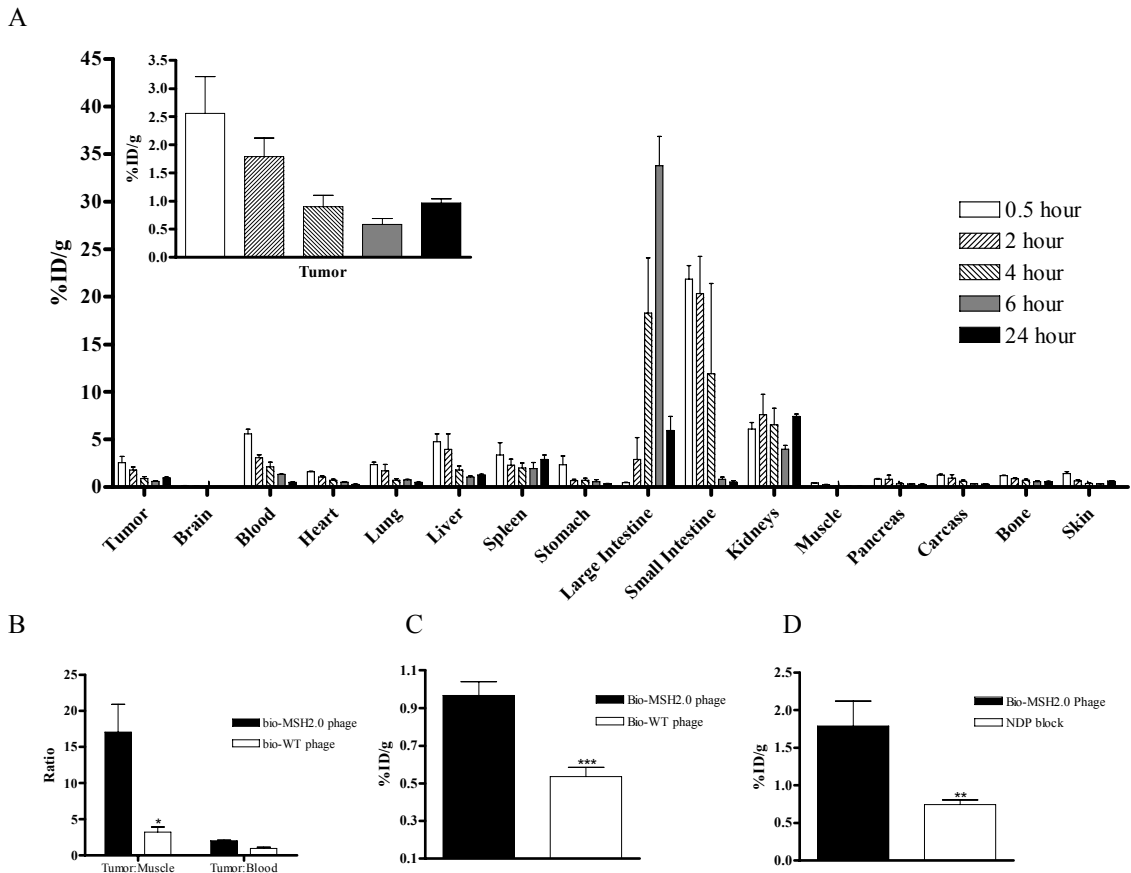
(A) C57/BL6 mice with syngeneic grafted B16-F1 melanoma tumors received a tail vein

injection of 5 x 10^{12} virions of bio-MSH2.0 phage. Four hours later the mice received a

tail vein injection of 1.85 MBq of ^{111}In-SA. The mice were then sacrificed at 0.5, 2, 4, 6,

and 24 hours post injection and their organs harvested for counting. (B) C57/BL6 mice

bearing B16-F1 tumors received tail vein injections of 5 x 10^{12} virions bio-WT phage

followed four hours later by 1.85 MBq of ^{111}In-SA. The tumor to muscle ratios and the

tumor to blood ratios for both the bio-MSH2.0 phage and bio-WT phage were then

compared. (C) 24 hours post injection of ^{111}In-SA the accumulation of radioactivity within the tumor was compared between bio-MSH2.0 phage and bio-WT phage. (D) C57/BL6 mice with syngeneic grafted B16-F1 melanoma tumor received a tail vein injection of either 5 x 10^{12} virions of bio-MSH2.0 phage or 5 x 10^{12} virions of bio-MSH2.0 phage mixed with 100 µg NDP. Four hours later the mice received a tail vein injection of 1.85 MBq of ^{111}In-SA. The mice were sacrificed at two hours post injection and accumulation of radiolabel within the tumor was compared to that of bio-MSH2.0 phage. (* 0.001=p; ** 0.002=p; ***0.003=p)

Figure 9: SPECT imaging of C57/BL6 mice bearing B16-F1 melanoma tumors.

Coregistered SPECT/CT image   Axial SPECT/CT
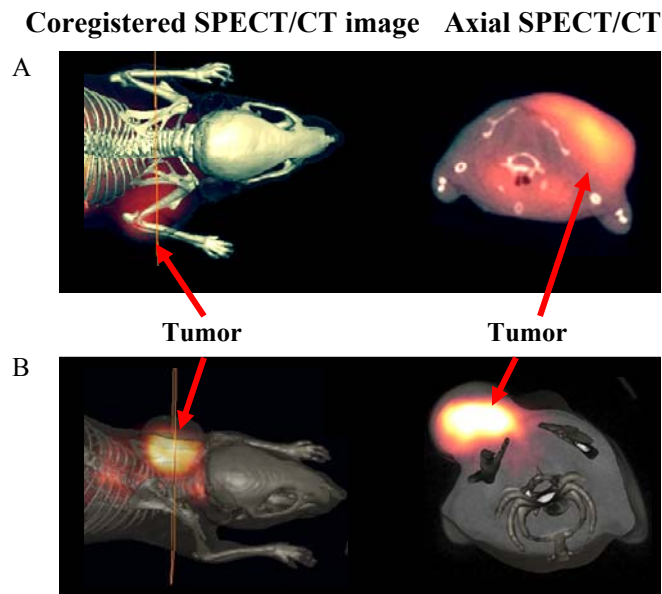
C57/BL6 mice with syngeneic grafted B16-F1 melanoma tumors received tail vein injections of 5 x 10^{12} virions of bio-MSH2.0 phage followed by an injection of 7.40 MBq ^{111}In-SA four hours later. The mice were sacrificed at 4 hours post injection and image data was acquired using a CTI-Concorde Microsystems Micro SPECT/CT System.

CHAPTER 4

SUMMARY

The purpose of these studies was to develop phage into agents useful for the *in vivo* imaging of cancer within tumor bearing mice. Each imaging modality utilized has its own set of advantages and disadvantages. Optical imaging with NIRF is still very new and will take a long time before it is introduced into the clinical setting. In comparison, SPECT imaging with gamma emitting radiolabels is a technique commonly utilized in both the laboratory and clinical setting. Unfortunately, phage possess a slow *in vivo* clearance profile (*13, 42*) and as such direct labeling of phage with radioisotopes would not be advisable due to harmful radiation-induced bystander effects (*14, 15*). Therefore, a two-step pretargeting strategy is necessary to evade potential harm to healthy tissues. In contrast the presence of NIRF poses no threat to healthy tissues and, as such, direct labeling of phage with NIRF is feasible.

In addition, use of phage as imaging agents has many advantages such as low cost, flexibility, *in vivo* stability and safety. However, the vector chosen for display of the peptide is an important consideration, as well as the chosen peptide itself. These studies utilized two different forms of displayed peptides, one selected within the fUSE5 vector and the other logically designed for placement within the fUSE5 vector. The inability to directly fuse the α-MSH targeting sequence to cpIII without altering the peptide/receptor ligand recognition demonstrates that conformational restraints are present and must be taken into consideration. One way to avoid these potential problems

would be to undergo phage display affinity maturation using the original core peptide sequence with randomized flanking sequence.

As stated earlier an advantage to the use of phage as an imaging agent for the *in vivo* imaging of cancer in tumor bearing mice is flexibility. Not only are phage easily manipulated to display different peptides, it is also simple to multiply label phage with molecules ranging from PEO_4-Biotin with a molecular weight of 474.59 daltons to the relatively large AF680 (molecular weight = 1150). Once labeled the complex remains stable, both *in vitro* and *in vivo* for long periods of time. The large size of the phage particles can provide the needed spatial separation of the targeting peptide and the label, thus, preventing masking of the peptide. These desirous attributes along with others make phage and phage display technology an attractive starting point for the generation of new cancer specific imaging agents.

In conclusion, these studies demonstrate the convenience and versatility of fd-filamentous phage for the delivery of tumor homing peptides and a diverse range of reporter molecules for the purpose of *in vivo* imaging of cancer.

REFERENCES

1. R. Twombly, *Journal of the National Cancer Institute* **97**, 330 (2005).
2. A. Jemal *et al.*, *CA: A Cancer Journal for Clinicians* **55**, 10 (Jan-Feb, 2005).
3. S. Williams-Brown, G. K. Singh, *Seminars in Oncology Nursing* **21**, 236 (Nov, 2005).
4. B. K. Kleinschmidt-Demasters, J. S. Kang, K. O. Lillehei, *Journal of Neuropathology and Experimental Neurology* **65**, 204 (Mar, 2006).
5. D. M. Brizel, *Seminars in Radiation Oncology* **8**, 237 (Oct, 1998).
6. G. S. Ginsburg, J. J. McCarthy, *Trends in Biotechnology* **19**, 491 (Dec, 2001).
7. R. C. Ladner, *Quarterly Journal of Nuclear Medicine* **43**, 119 (1999).
8. S. F. Parmley, G. P. Smith, *Gene* **73**, 305 (1988).
9. L. X. Wang, J. Ni, S. Singh, *Bioorganic and Medicinal Chemistry* **11**, 159 (Jan 2, 2003).
10. R. J. Kok *et al.*, *Bioconjugate Chemistry* **13**, 128 (Jan-Feb, 2002).
11. J. C. Reubi, *Endocrine Reviews* **24**, 389 (Aug, 2003).
12. S. Guccione, K. C. Li, M. D. Bednarski, *IEEE Engineering in Medicine and Biology Magazine* **23**, 50 (Sep-Oct, 2004).
13. C. J. Inchley, *Clinical and Experimental Immunology* **5**, 173 (1969).
14. H. B. Stone, W. H. McBride, C. N. Coleman, *Radiation Research* **157**, 204 (Feb, 2002).
15. C. Mothersill, C. B. Seymour, *Nat Rev Cancer* **4**, 158 (Feb, 2004).
16. B. W. Rice, M. D. Cable, M. B. Nelson, *Journal of Biomedical Optics* **6**, 432 (Oct, 2001).
17. N. C. Shaner *et al.*, *Nature Biotechnology* **22**, 1567 (Dec, 2004).
18. Y. Lin, R. Weissleder, C. H. Tung, *Bioconjugate Chemistry* **13**, 605 (May-Jun, 2002).
19. B. R. Renikuntla, H. C. Rose, J. Eldo, A. S. Waggoner, B. A. Armitage, *Org Lett* **6**, 909 (Mar 18, 2004).
20. S. A. Hilderbrand, K. A. Kelly, R. Weissleder, C. H. Tung, *Bioconjugate Chemistry* **16**, 1275 (Sep-Oct, 2005).
21. E. E. Graves, R. Weissleder, V. Ntziachristos, *Curr Mol Med* **4**, 419 (Jun, 2004).
22. V. Ntziachristos *et al.*, *Proceedings of the National Academy of Sciences of the United States of America* **101**, 12294 (Aug 17, 2004).
23. T. C. Doyle, S. M. Burns, C. H. Contag, *Cellular Microbiology* **6**, 303 (Apr, 2004).
24. A. Rehemtulla *et al.*, *Neoplasia (New York)* **2**, 491 (Nov-Dec, 2000).
25. M. Edinger *et al.*, *Neoplasia (New York)* **1**, 303 (Oct, 1999).
26. V. Ntziachristos, A. G. Yodh, M. Schnall, B. Chance, *Proceedings of the National Academy of Sciences of the United States of America* **97**, 2767 (Mar 14, 2000).
27. O. C. Boerman, F. G. van Schaijk, W. J. Oyen, F. H. Corstens, *Journal of Nuclear Medicine* **44**, 400 (Mar, 2003).
28. G. Paganelli *et al.*, *European Journal of Nuclear Medicine* **19**, 322 (1992).
29. D. M. Goldenberg, R. M. Sharkey, *Q J Nucl Med Mol Imaging* **50**, 248 (Dec, 2006).

30. C. f. D. Control, *www.cdc.gov/cancer/prostate/prostate.htm* (2003).

31. M. A. Poul, B. Becerril, U. B. Nielsen, P. Morisson, J. D. Marks, *Journal of Molecular Biology* **301**, 1149 (2000).

32. N. Karasseva, V. V. Glinsky, N. X. Chen, R. Komatireddy, T. P. Quinn, *Journal of Protein Chemistry* **21**, 287 (2002).

33. E. N. Peletskaya, V. V. Glinsky, G. V. Glinsky, S. L. Deutscher, T. P. Quinn, *Journal of Molecular Biology* **270**, 374 (1997).

34. K. A. Kelly, D. A. Jones, *Neoplasia (New York)* **5**, 437 (September/Oct 2003, 2003).

35. V. I. Romanov, D. B. Durand, V. A. Petrenko, *Prostate* **47**, 239 (2001).

36. W. Arap, R. Pasqualini, E. Ruoslahti, *Science* **279**, 377 (Jan 16, 1998).

37. R. Pasqualini, E. Ruoslahti, *Nature* **380**, 364 (1996).

38. G. P. Smith, *Science* **228**, 1315 (Jun 14, 1985).

39. M. E. Kaighn, K. S. Narayan, Y. Ohnuki, J. F. Lechner, L. W. Jones, *Investigative Urology* **17**, 16 (1979).

40. G. P. Smith, *Science.* **228**, 1315.

41. G. P. Smith. (University of Missouri-Columbia).

42. J. Zou, M. T. Dickerson, N. K. Owen, L. A. Landon, S. L. Deutscher, *Molecular Biology Reports* **37**, 121 (2004 Jan).

43. J. M. Rini, Y. D. Lobsanov, *Current Opinion in Structural Biology* **9**, 578 (1999).

44. S. F. Altschul *et al.*, *Nucleic Acids Research* **25**, 3389 (Sep 1, 1997).

45. D. G. George, W. C. Barker, H. W. Mewes, F. Pfeiffer, A. Tsugita, *Nucleic Acids Research* **24**, 17 (Jan 1, 1996).

46. L. A. Landon *et al.*, *Journal of Protein Chemistry* **22**, 193 (2003).

47. J. R. Newton, K. A. Kelly, U. Mahmood, R. Weissleder, S. L. Deutscher, *Neoplasia (New York)* **8**, 772 (2006).

48. H. Moriyama, H. Nakano, M. Igawa, H. Nihira, *Urologia Internationalis* **42**, 120 (1987).

49. R. J. Giordano, M. Cardo-Vila, J. Lahdenranta, R. Pasqualini, W. Arap, *Nature Medicine.* **7**, 1249.

50. M. A. Spear *et al.*, *Cancer Gene Therapy.* **8**, 506.

51. N. B. Adey, A. H. Mataragnon, J. E. Rider, J. M. Carter, B. K. Kay, *Gene* **156**, 27 (Apr 14, 1995).

52. C. R. Merril, D. Scholl, S. L. Adhya, *Nature Reviews Drug Discovery* **2**, 489 (Jun, 2003).

53. K. Kelly, H. Alencar, M. Funovics, U. Mahmood, R. Weissleder, *Cancer Research* **64**, 6247 (Sep 1, 2004).

54. E. Koivunen, B. Wang, E. Ruoslahti, *Journal of Cell Biology* **124**, 373 (Feb, 1994).

55. H. Burke, *Cancer Informatics* **1**, 15 (2005).

56. C. Mao *et al.*, *Proceedings of the National Academy of Sciences of the United States of America* **100**, 6946 (Jun 10, 2003).

57. J. Lovric *et al.*, *Journal of Molecular Medicine* **83**, 377 (May, 2005).

58. A. Shiohara, A. Hoshino, K. Hanaki, K. Suzuki, K. Yamamoto, *Microbiology and Immunology* **48**, 669 (2004).

59. E. B. Voura, J. K. Jaiswal, H. Mattoussi, S. M. Simon, *Nature Medicine* **10**, 993 (Sep, 2004).
60. B. Ballou, B. C. Lagerholm, L. A. Ernst, M. P. Bruchez, A. S. Waggoner, *Bioconjugate Chemistry* **15**, 79 (Jan-Feb, 2004).
61. L. A. Landon, J. Zou, S. L. Deutscher, *Molecular Diversity* **8**, 35 (2004, 2003).
62. R. J. Giordano, M. Cardo-Vila, J. Lahdenranta, R. Pasqualini, W. Arap, *Nature Medicine* **7**, 1249 (Nov, 2001).
63. Z. Li *et al.*, *FASEB Journal* **19**, 1978 (Dec, 2005).
64. B. Dreier *et al.*, *Journal of Biological Chemistry* **280**, 35588 (Oct 21, 2005).
65. L. A. Landon, J. Zou, S. L. Deutscher, *Curr Drug Discov Technol* **1**, 113 (Jun, 2004).
66. T. Mori, *Current Pharmaceutical Design* **10**, 2335 (2004).
67. X. Chen *et al.*, *Neoplasia (New York)* **7**, 271 (Mar, 2005).
68. S. J. Kennel *et al.*, *Nuclear Medicine and Biology* **27**, 815 (2000).
69. D. L. Jaye, C. M. Geigerman, R. E. Fuller, A. Akyildiz, C. A. Parkos, *Journal of Immunological Methods* **295**, 119 (Dec, 2004).
70. J. Zou, M. T. Dickerson, N. K. Owen, L. A. Landon, S. L. Deutscher, *Molecular Biology Reports* **31**, 121 (Jun, 2004).
71. W. Siegrist *et al.*, *Cancer Research* **49**, 6352 (Nov 15, 1989).
72. R. D. Cone *et al.*, *Annals of the New York Academy of Sciences* **680**, 342 (May 31, 1993).
73. J. B. Tatro *et al.*, *Journal of Clinical Investigation* **85**, 1825 (Jun, 1990).
74. D. S. Wilbur, D. K. Hamlin, J. Sanderson, Y. Lin, *Bioconjugate Chemistry* **15**, 1454 (Nov-Dec, 2004).
75. T. K. Sawyer *et al.*, *Proceedings of the National Academy of Sciences of the United States of America* **77**, 5754 (Oct, 1980).
76. J. Chen, M. F. Giblin, N. Wang, S. S. Jurisson, T. P. Quinn, *Nuclear Medicine and Biology* **26**, 687 (1999).
77. S. Froidevaux, M. Calame-Christe, H. Tanner, A. N. Eberle, *Journal of Nuclear Medicine* **46**, 887 (May, 2005).
78. J. Chen, Z. Cheng, T. J. Hoffman, S. S. Jurisson, T. P. Quinn, *Cancer Research* **60**, 5649 (Oct 15, 2000).
79. Z. Cheng *et al.*, *Journal of Medicinal Chemistry* **45**, 3048 (2002).
80. Limor Chen, B. Schechter, R. Arnon, M. Wilchek, *Drug Development Research* **50**, 258 (2000).
81. D. S. Wilbur *et al.*, *Bioconjugate Chemistry* **9**, 322 (May-Jun, 1998).
82. B. Schechter, R. Silberman, R. Arnon, M. Wilchek, *European Journal of Biochemistry* **189**, 327 (Apr 30, 1990).
83. R. E. Weiner, M. L. Thakur, *BioDrugs* **19**, 145 (2005).